Neuroscience

Rab10 inactivation promotes AMPAR trafficking and spine enlargement during long-term potentiation

Jie Wang, Jun Nishiyama, Paula Parra-Bueno, Elwy Okaz, Goksu Oz, Xiaodan Liu, Tetsuya Watabe, Irena Suponitsky-Kroyter, Timothy E McGraw, Erzsebet M Szatmari, Ryohei Yasuda

Department of Neurobiology, Duke University School of Medicine, Durham, United States • Neuronal Signal Transduction Group, Max Planck Florida Institute for Neuroscience, Jupiter, United States • Division of Life Science, The Hong Kong University of Science and Technology, Hong Kong, China • Program in Neuroscience and Behavioral Disorders, Duke-NUS Medical School, Singapore, Singapore • Weill Cornell Medicine Graduate School of Medical Sciences, New York, United States • Department of Physical Therapy, East Carolina University, Greenville, United States

Reviewed Preprint
v2 • March 6, 2025
Revised by authors

Reviewed Preprint
v1 • December 11, 2024

eLife Assessment

This is an **important** study that describes the development of optical biosensors for various Rab GTPases and explores the contributions of Rab10 and Rab4 to structural and functional plasticity at hippocampal synapses during glutamate uncaging. The evidence supporting the conclusions of the paper is **solid**, and several improvements were noted by the reviewers upon revision, although some persisting inconsistencies would benefit from further clarification.

https://doi.org/10.7554/eLife.103879.2.sa4

Abstract

Summary

Rab-dependent membrane trafficking is critical for changing the structure and function of dendritic spines during synaptic plasticity. Here, we developed highly sensitive sensors to monitor Rab protein activity in single dendritic spines undergoing structural long-term potentiation (sLTP) in rodent organotypic hippocampal slices. During sLTP, Rab10 was persistently inactivated (>30 min) in the stimulated spines, whereas Rab4 was transiently activated over ~5 min. Inhibiting or deleting Rab10 enhanced sLTP, electrophysiological LTP and AMPA receptor (AMPAR) trafficking during sLTP. In contrast, disrupting Rab4 impaired sLTP only in the first few minutes, and decreased AMPAR trafficking during sLTP. Thus, our results suggest that Rab10 and Rab4 oppositely regulate AMPAR trafficking during sLTP, and inactivation of Rab10 signaling facilitates the induction of LTP and associated spine structural plasticity.

Introduction

Structural long-term potentiation (sLTP) is the structural basis of long-term potentiation (LTP) and plays a critical role in learning and memory[1–3]. Upon electrical synaptic stimulation or glutamate uncaging, Ca^{2+} influx through NMDA-type glutamate receptors (NMDARs) into dendritic spines triggers diverse downstream signaling cascades, including Ca^{2+}/calmodulin-dependent protein kinase II (CaMKII) and extracellular signal-regulated kinase (ERK), which lead to the increase in spine volume and synaptic efficacy[4,5]. sLTP has two distinct phases: it starts with a rapid and transient spine enlargement over the first few minutes (transient phase), followed by a sustained enlargement over hours (sustained phase)[3,6]. Different pharmacological or genetic manipulations can selectively inhibit these two phases, indicating distinct induction mechanisms[6]. The sustained phase is known to be coupled with LTP, while the physiological role of the transient phase is less clear[3,6]. Nevertheless, the transient phase is associated with the rapid ultrastructural changes of PSD and surrounding membrane and thus may be important for the dramatic synaptic increase in the initial phase of sLTP[7]. In addition, the spine enlargement during the transient phase induces presynaptic potentiation through mechanical force by pushing on the presynaptic bouton[8].

During LTP and sLTP, various internal membranes are exocytosed in dendrites in an activity-dependent manner to add spine membrane area, increase surface glutamate receptors, and release plasticity-related peptides[9–13]. Particularly, activity-dependent synaptic delivery of GluA1 subunit of AMPA-type glutamate receptor (AMPAR) is considered one of the major mechanisms to increase postsynaptic glutamate sensitivity during LTP[14–18]. Several members of the postsynaptic exocytosis machinery have been identified, including the soluble NSF-attachment protein receptor (SNARE) proteins, complexin, synaptotagmins, and myosin Vb[12,19–24].

Among the molecules regulating intracellular trafficking, Rab GTPases constitute the largest Ras subfamily, with more than 60 members localized to distinct intracellular domains[25,26]. As small GTPases, Rab proteins switch between two states, the guanosine-5'-triphosphate (GTP)-bound "active" state and the guanosine diphosphate (GDP)-bound "inactive" state. Specific guanine nucleotide exchange factors (GEFs) and GTPase activating proteins (GAPs) regulate the conversion between these two states[25]. Once activated, Rab GTPases recruit diverse downstream effectors to coordinate intracellular transport during vesicle budding, movement, tethering, and fusion[27]. Several members of Rab GTPases have been shown to coordinate AMPAR trafficking during synaptic plasticity[28]. Rab8 and Rab11 regulate the exocytosis of AMPARs during LTP[29–31], whereas Rab5 drives the endocytosis of AMPARs during long-term depression (LTD)[32]. Rab4 is dispensable for LTP but is required for the maintenance of spine morphology[29]. Rab4 also regulates both the fast and slow endosomal recycling to the plasma membrane[33–35]. However, the function of other Rabs in synaptic plasticity is little known. Notably, Rab10 is expressed in dendrites[36–39] and has been implicated in Alzheimer's disease resilience[40,41]. Thus, Rab10 is potentially involved in membrane trafficking during synaptic plasticity.

In the present study, we developed a general design of FRET/FLIM-based sensors for various Rab proteins. Among these sensors, we further focused on the spatiotemporal dynamics of Rab10 and Rab4 activity during sLTP. We found that postsynaptic stimulation leads to the persistent inactivation of Rab10 and transient activation of Rab4 in spines undergoing sLTP. These Rab activity changes are dependent on NMDAR and CaMKII activation. Moreover, knock-down analyses demonstrate that Rab10 serves as a negative regulator of sLTP, whereas Rab4 contributes to the transient phase of sLTP. In addition, postnatal deletion of Rab10 from excitatory neurons enhanced sLTP and electrophysiological LTP at Schaeffer collateral pathway. Furthermore, Rab10 negatively regulates activity-dependent GluA1 trafficking into the stimulated spines during sLTP,

while Rab4 positively controls this process. Therefore, our results suggest that Rab10 inhibits AMPAR trafficking during synaptic potentiation and NMDAR-dependent inactivation of Rab10 facilitates LTP induction. On the contrary, Rab4 promotes AMPAR trafficking during sLTP and NMDAR-dependent activation of Rab4 regulates the transient phase of sLTP.

Results

Highly sensitive and selective FRET sensors for Rab proteins

To image Rab signaling activity in single dendritic spines, we developed FRET sensors for Rab4, 5, 7, 8, and 10. The Rab sensors have two components: (1) the Rab protein tagged with a fluorescent protein that serves as a FRET donor (monomeric enhanced green fluorescent protein (mEGFP)-Rab or mTurquoise2-Rab) and (2) a Rab binding domain (RBD) from a specific effector protein that is tagged with two fluorescent proteins as FRET acceptors (mCherry-RBD-mCherry or mVenus-RBD-mVenus). When the Rab protein is activated, RBD and Rab increase their binding and thus increase FRET between the donor and acceptor fluorophores (**Fig. 1a**). The fraction of Rab bound to the RBD (binding fraction) was calculated by measuring the fluorescence lifetime of the donor[42,43].

For Rab4, 5, 7, 8 and 10, we used Rabenosyn5 [439-503], EEA1 [36-128], FYCO1 [963-206], Rim2 [27-175] and Rim1 [20-277] as RBDs, respectively[44–47]. To test the sensitivity and specificity of these Rab sensors, we took three approaches. First, we transfected wild-type (WT)-Rab, dominant-negative (DN)-Rab, and constitutively active (CA)-Rab sensors in HEK 293T cells. As expected, DN-Rab and CA-Rab sensors displayed lower and higher binding fractions than the WT-Rab sensor, respectively, indicating the sensitivity of Rab sensors (**Fig. 1b,c**). Particularly, Rab4 and Rab10 sensors showed significantly different binding fractions between WT- and DN- or CA-Rabs (**Fig. 1b,c**). For Rab10 sensor, we used the mTurquoise2-mVenus pair instead of the mEGFP-mCherry pair since it reported higher binding fraction differences between WT- and DN-, as well as WT-and CA-Rab10 sensors in HEK 293T cells (**Fig. 1b,c**, **Extended Data Fig. 1a-d**)[48,49]. Second, we coexpressed a Rab sensor with the corresponding Rab GAPs or GEFs to test whether the sensor could respond to the known upstream signaling[50–56]. Indeed, these GAPs and GEFs respectively decreased and increased the activity of Rab proteins as reported by the sensor (**Fig. 1d-I**). Compared with Rab5 and Rab8, Rab4, Rab7 and Rab10 sensors displayed higher binding fraction changes in response to GAPs or GEFs (**Fig. 1d-i**). Third, we measured Rab activity change in response to N-Methyl-D-aspartic acid (NMDA) application in neurons[6]. We biolistically transfected rat organotypic hippocampal slices with each Rab sensor and imaged the proximal apical dendrites of CA1 pyramidal neurons. Bath application of NMDA (15 μM, 2 min) in zero extracellular Mg^{2+} triggered a robust activation of Rab sensors in the dendrites, suggesting that Rab sensors could report neuronal Rab activities (**Fig. 1j**). Nevertheless, these Rab sensors showed different activation kinetics upon NMDA stimulation (**Fig. 1j** and **Extended Data Fig. 1e**). Rab4 sensor was rapidly activated, peaked at 3 min and subsequently decayed (**Fig. 1j** and **Extended Data Fig. 1e**). On the contrary, Rab5, 7, 8 and 10 sensors displayed a gradually accumulated activation pattern, which peaked at 6-11 min and decreased afterwards (**Fig. 1j** and **Extended Data Fig. 1e**). Notably, Rab10 sensor was transiently inactivated in the first 2 min, possibly reflecting a fast response to NMDAR activation (**Fig. 1j** and **Extended Data Fig. 1e**). Overall, these results demonstrate that our Rab sensor strategy is generalizable to many Rab proteins.

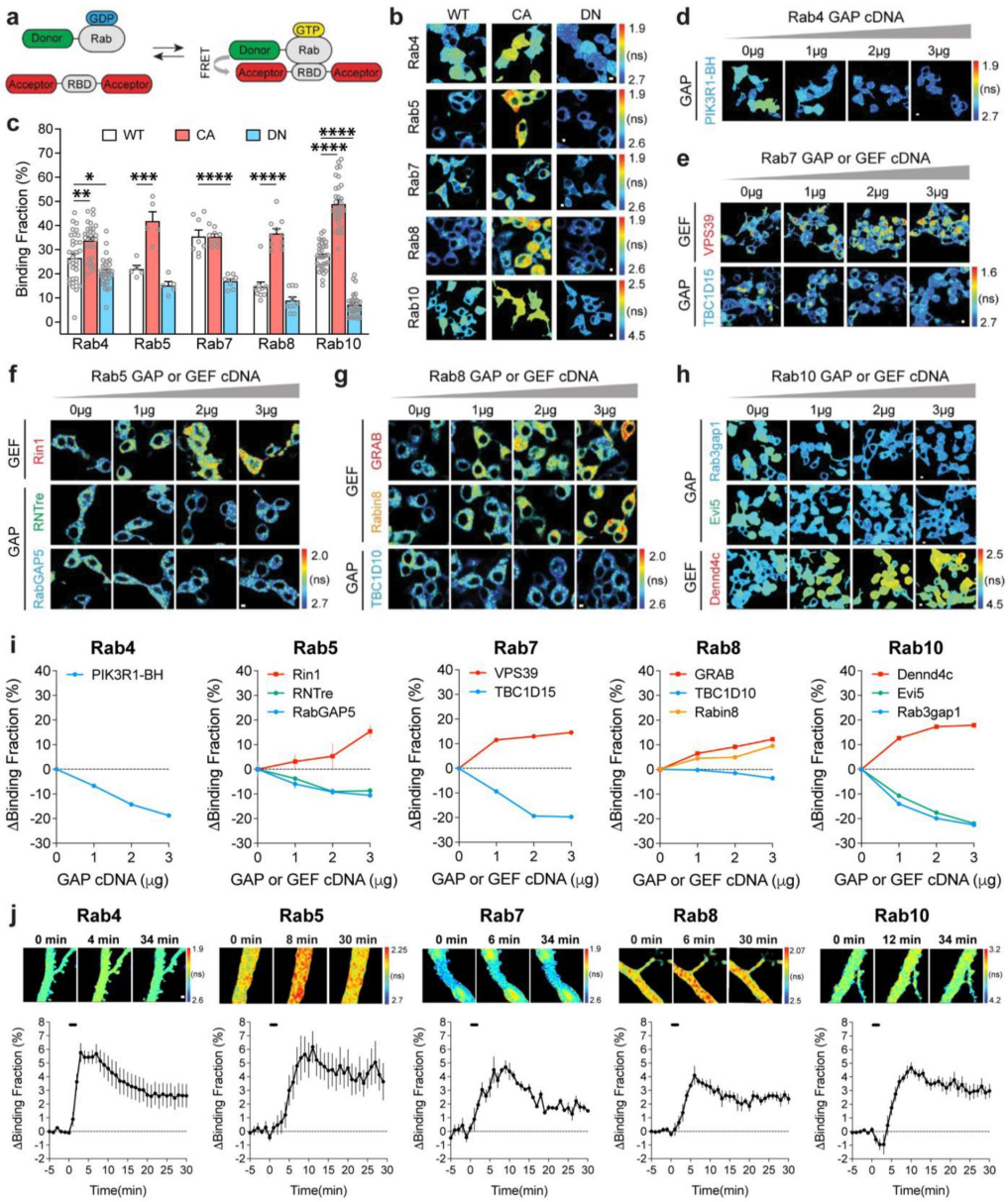

Fig. 1

Design and characterizations of Rab FRET sensors.

a, Schematic diagrams illustrating the FRET sensor design for Rab proteins. RBD: Rab binding domain; GDP: guanosine diphosphate; GTP: guanosine-5'-triphosphate. **b**, Representative fluorescence lifetime images of HEK 293T cells transfected with Rab wild type (WT), dominant negative (DN, Rab4 [S27N], Rab5 [S34N], Rab7 [T22N], Rab8 [S22N] and Rab10 [T23N]) and constitutively active (CA, Rab4 [Q72L], Rab5 [Q79L], Rab7 [Q67L], Rab8 [Q67L] and Rab10 [Q68L]) sensors. FRET donor/acceptor pair is mEGFP/mCherry for Rab4, 5, 7 and 8; for Rab10, FRET donor/acceptor pair is mTurquoise2/mVenus. Warmer color indicates shorter lifetime and higher activity. Scale bars represent 5 μm. **c**, Quantification of binding fraction for experiments in b. Data represent mean ± SEM. N=5-32. One-way ANOVA followed by Bonferroni's multiple comparison tests were performed (* p<0.05, ** p<0.01, *** p<0.001, **** p<0.0001). **d-h**, Representative fluorescence lifetime images of individual Rab wild type sensor cotransfected with the corresponding GAP (green and blue) or GEF (red and orange) cDNAs. Scale bars represent 5 μm. **i**, Quantification of binding fraction change for experiments in d-h. N=5-20. Data represent mean ± SEM. **j**, Activation of Rab sensors by NMDA application in rat hippocampal CA1 pyramidal neurons. Upper: representative fluorescence lifetime images of Rab sensor-expressing neurons in response to bath application of 15 μM NMDA for 2 min. Scale bar is 1 μm. Lower: quantification of binding fraction change for upper lane experiments. Data represent mean ± SEM. N=4-11 for each group.

Rab10 is persistently inactivated in the stimulated spines during sLTP

We biolistically transfected cultured organotypic hippocampal slices of rats with Rab10 sensor, and imaged the secondary apical dendrites of CA1 pyramidal neurons. mTurquoise2-Rab10, the sensor donor, was continuously distributed in the dendrites and spines, without showing an endosomal punctate pattern (**Fig. 2a**). To eliminate the effect of protein overexpression on its localization, we probed endogenous Rab10 by CRISPR-Cas9-mediated homology-directed repair (SLENDR) technique *in vivo* (**Extended Data Fig. 1f-j**)[59]. Endogenous Rab10 displayed a heterogeneous pattern: it is widely distributed along the dendrite and protrudes into the spines (**Extended Data Fig. 1i**). To elucidate the subcellular compartmentalization of Rab10, we further examined its colocalization with exogenously expressed endosomal markers *in vivo* (**Extended Data Fig. 1j**). Rab10 is significantly overlapped with Rab7-labelled lysosomes, partially colocalized with Rab11-labelled recycling endosomes, but separated from Rab5-labelled early endosomes (**Extended Data Fig. 1j**).

To characterize the spatiotemporal dynamics of Rab10 activity in single dendritic spines during sLTP, we combined two-photon glutamate uncaging with 2pFLIM[6,13,57,58], and imaged the secondary apical dendrites of CA1 pyramidal neurons expressing the Rab10 sensor at 25-27°C. Upon focal glutamate uncaging (0.5 Hz, 60 s) in zero extracellular Mg^{2+}, a single spine underwent a rapid volume increase within the first few minutes ($\Delta V_{transient}$ = 275.9 ± 25.0%; **Fig. 2a,e,f**), which decayed to a smaller but sustained volume increase lasting more than 30 min ($\Delta V_{sustained}$ = 79.6 ± 6.7%; **Fig. 2a,e,g**), consistent with the previous studies[3,6,13,57,58]. Concomitant with the spine enlargement, Rab10 showed a rapid and spine-specific decrease of activity in the stimulated spines, which lasted for more than 30 min (**Fig. 2a-d**). Neither the changes in spine volume, basal binding fraction nor the changes in the binding fraction of Rab10 sensor correlated with the initial spine size (**Extended Data Fig. 2a-e**). To verify the specificity of the sensor response, we replaced the RBD of the Rab10 sensor with the RBD of Rab4 sensor (Rabenosyn5 [439-503], false acceptor). This false acceptor sensor did not show a significant change in FRET (measured as the binding fraction change) in the stimulated spines (**Fig. 2c,d,f,g** and **Extended Data Fig. 3**). In addition, the Rab10 sensor displayed a similar inactivation pattern at a near physiological temperature (33-35°C; **Extended Data Fig. 4**). In summary, our results demonstrate that Rab10 is persistently inactivated in the stimulated spines during sLTP, and this inactivation is compartmentalized in the stimulated spines.

The persistent inactivation of Rab10 during sLTP may be caused by the dilution of active Rab10 proteins due to the rapid spine enlargement. To examine this possibility, we compared the basal binding fraction of Rab10 sensor in spines and dendrites, and analyzed the subset of spines with lower Rab10 basal activity than the dendrite (**Extended Data Fig. 5b-d**). We found that Rab10 activity still decreased against the gradient at the spine neck upon sLTP induction (**Fig. 2** and **Extended Data Fig. 5d**). In addition, binding fraction of Rab10 sensor is independent of donor intensity (**Extended Data Fig. 5a**). Thus, instead of passive signal dilution, the persistent inactivation of Rab10 requires active biological processes, presumably by translocating Rab10 positive vesicles out of the spine or directly inactivating Rab10 in the spine. To examine whether Rab10 distribution is changed during sLTP, we further analyzed the intensity of Rab10 donor in the stimulated spines and dendrites. Upon sLTP induction, Rab10 donor intensity significantly increased in the stimulated spines but remained unchaged in the dendrites (**Extended Data Fig. 6a**). The dramatic increase of Rab10 intensity in the stimulated spines was probably due to passive diffusion by spine enlargement. Therefore, we further analyzed the mean intensities of Rab10 donor in the stimulated spines and dendrites, which were similar prior and post sLTP induction (**Extended Data Fig. 6b,c**).

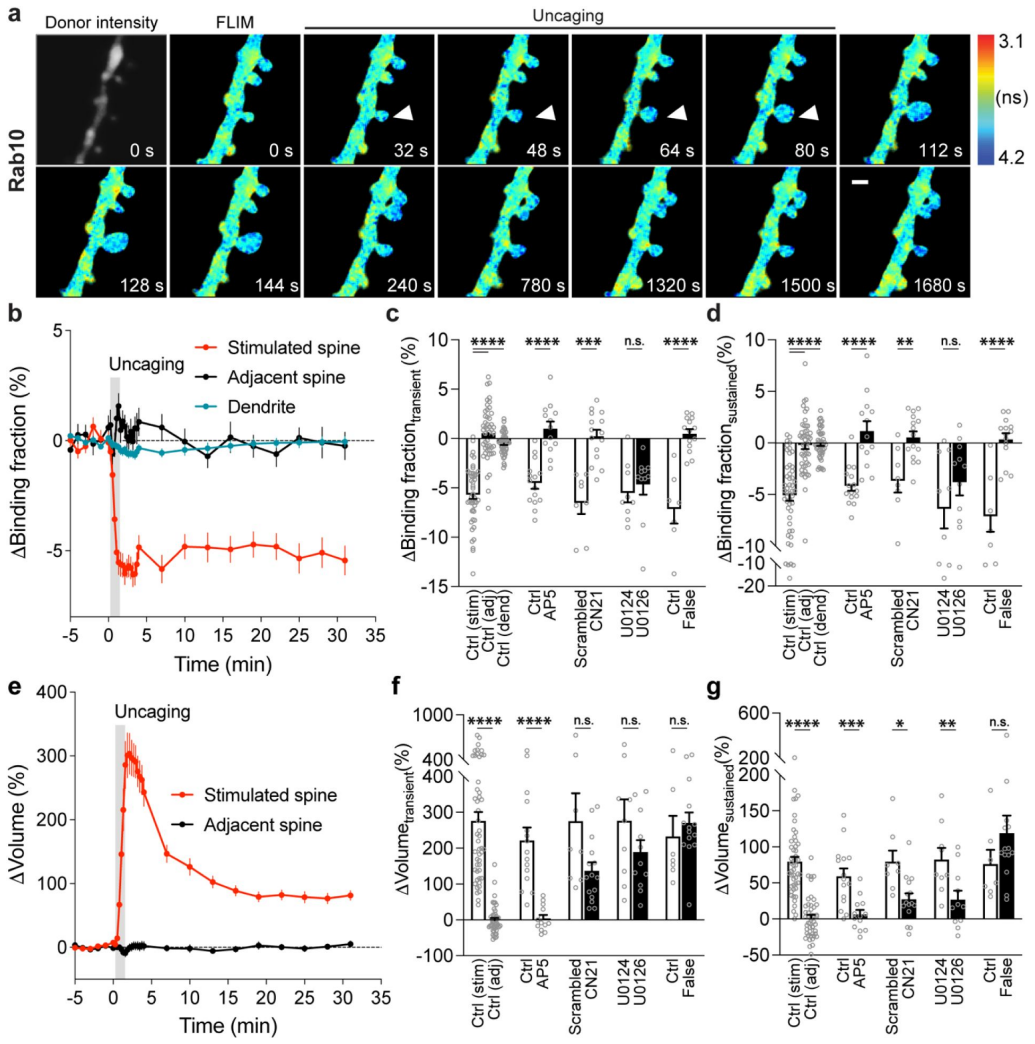

Fig. 2

Spatiotemporal dynamics of Rab10 inactivation during sLTP in single spines.

a, Representative donor fluorescence intensity image (gray) and fluorescence lifetime (FLIM, colorful) images of Rab10 inactivation during sLTP induced by two-photon glutamate uncaging. Arrowheads indicate the stimulated spine. The colder color indicates longer lifetime and lower Rab10 activity. Scale bar represents 1 μm. **b,** Averaged time courses of Rab10 inactivation measured as binding fraction changes between mTurquoise2-Rab10 and mVenus-Rim1 [20-277]-mVenus in the stimulated spine (red), adjacent spine (black) and dendrite (blue). Grey rectangle bar indicates glutamate uncaging (0.5 Hz, 60 s). Data are presented in mean ± SEM. N=49/42 (spine/neuron), 49/42 (spine/neuron) and 49/42 (dendrite/neuron) for the stimulated spine, adjacent spine and dendrite, respectively. **c,d**, Quantification of Rab10 binding fraction changes in the transient phase (c, averaged over 1.3-4 min) and sustained phase (d, averaged over 19-31 min) in the stimulated spine (stim), adjacent spine (adj) and dendrite (dend) for the same experiments as b. Data represent mean ± SEM. One-way ANOVA followed by Bonferroni's multiple comparison tests were performed for the stimulated spine, adjacent spine and dendrite (**** p<0.0001). Effects of pharmacological agents on Rab10 inactivation in the stimulated spines are also presented. All pharmacological inhibition experiments were paired with controls from the same batch of slices. Data represent mean ± SEM. Student's t-tests were performed (n.s., not significant, ** p<0.01, *** p<0.001, **** p<0.0001). N=15/14, 13/11, 8/7, 15/12, 9/8 and 11/8 (spine/neuron) for Ctrl, AP5, scrambled, CN21, U0124 and U0126, respectively. When mTurquoise2-Rab10 was paired with a false acceptor (False), mVenus-Rabenosyn5 [439-503]-mVenus, little activity change was observed. Data represent mean ± SEM. Student's t-tests were performed (**** p<0.0001). N=7/7 and 14/9 (spine/neuron) for Ctrl and False, respectively. **e,** Averaged time courses of spine volume change in the same experiment as b. Data represent mean ± SEM. **f,g**, Quantification of spine volume changes in the transient phase (f, averaged over 1.3-4 min) and sustained phase (g, averaged over 19-31 min) for the same experiments as c and d. Data represent mean ± SEM. Student's t-tests were used for all groups (n.s., not significant, * p<0.05, ** p<0.01, *** p<0.001, **** p<0.0001).

To further identify signaling pathways that inactivate Rab10 during sLTP, we applied pharmacological inhibitors targeting potential upstream components[4,57]. Inhibition of NMDARs by 2-amino-5-phosphonopentanoic acid (AP5, 50 μM) completely abolished Rab10 inactivation and spine enlargement (**Fig. 2c,d,f,g** and **Extended Data Fig. 7a,b**). Application of CN21 (10 μM), a CaMKII inhibitory peptide[60,61], abolished Rab10 inactivation while partially attenuating the volume change (**Fig. 2c,d,f,g** and **Extended Data Fig. 7c,d**). In contrast, mitogen-activated protein kinase (MAPK)/ERK kinase (MEK) inhibitor U0126 (20 μM) had no effect on Rab10 inactivation, although it impaired sLTP during the sustained phase (**Fig. 2c,d,f,g** and **Extended Data Fig. 7e,f**). These results demonstrate that Rab10 is persistently inactivated in the stimulated spines during sLTP, and this inactivation is dependent on NMDARs and CaMKII but not on the MAPK/ERK signaling pathway.

Rab4 is transiently activated in the stimulated spines during sLTP

Next, we measured the spatiotemporal profile of Rab4 activity in dendrites during sLTP induced in single spines. Consistent with its localization in early and recycling endosomes[33–35], mEGFP-Rab4, the sensor donor, showed a punctate distribution pattern (**Fig. 3a**). In the basal state, Rab4 sensor activity is not correlated with the donor intensity, and was lower in the spines than dendrites (**Extended Data Fig. 5e-g**). Glutamate uncaging (0.5 Hz, 60 s) induced a transient and sustained volume increase in the stimulated spines of neurons expressing Rab4 sensor ($\Delta V_{transient}$ = 341.0 ± 29.4% and $\Delta V_{sustained}$ = 77.6 ± 8.0%; **Fig. 3a,e**-g). In contrast to the persistent inactivation of Rab10, Rab4 activity was transiently elevated in the stimulated spines and decayed, with no activity change in the adjacent spines or dendrites (**Fig. 3a-d**). This enhanced spine activity exceeds that of dendrite during sLTP, suggesting that the activation requires active processes (**Extended Data Fig. 5h**). Similarly to Rab10, we examined the intensity and mean intensity of Rab4 donor in the stimulated spines and dendrites. In the transient phase of sLTP, both the intensity and mean intensity of Rab4 donor significantly increased in the stimulated spines, suggesting recruitment of Rab4 into the stimulated spines (**Extended Data Fig. 6d-f**). In contrast, there was no donor intensity or mean intensity change in the dendrites (**Extended Data Fig. 6d-f**). Moreover, the initial spine volume was not correlated either with the volume changes, the basal activity of Rab4 reported or the level of Rab4 activation reported by the sensor (**Extended Data Fig. 2f-j**). Replacing the RBD of Rab4 sensor with the RBD for Rab10 sensor (Rim1 [20-227], false acceptor) showed no change of the binding fraction in the stimulated spines during sLTP, indicating the specificity of the sensor response (**Fig. 3c,d,f,g** and **Extended Data Fig. 8**). In addition, the Rab4 sensor showed a similar transient activation pattern at a near-physiological temperature (33-35°C; **Extended Data Fig. 9**). Thus, our results demonstrate that Rab4 is transiently activated in the stimulated spines during sLTP, and this activation is compartmentalized in the stimulated spines.

To identify signaling pathways that activate Rab4 during sLTP, we applied pharmacological inhibitors targeting putative upstream components. Inhibition of NMDARs by AP5 (50 μM) completely abolished Rab4 activation and spine enlargement (**Fig. 3c,d,f,g** and **Extended Data Fig. 10a,b**). Application of CN21 (10 μM) decreased Rab4 activity and volume changes both in the transient phase and sustained phase (**Fig. 3c,d,f,g** and **Extended Data Fig. 10c,d**). In contrast, MEK inhibitor U0126 (20 μM) had no effect on Rab4 activation, although it impaired sLTP during the sustained phase (**Fig. 3c,d,f,g** and **Extended Data Fig. 10e,f**). Altogether, Rab4 activation during sLTP is dependent on NMDARs and CaMKII, but not on the MAPK/ERK signaling pathway.

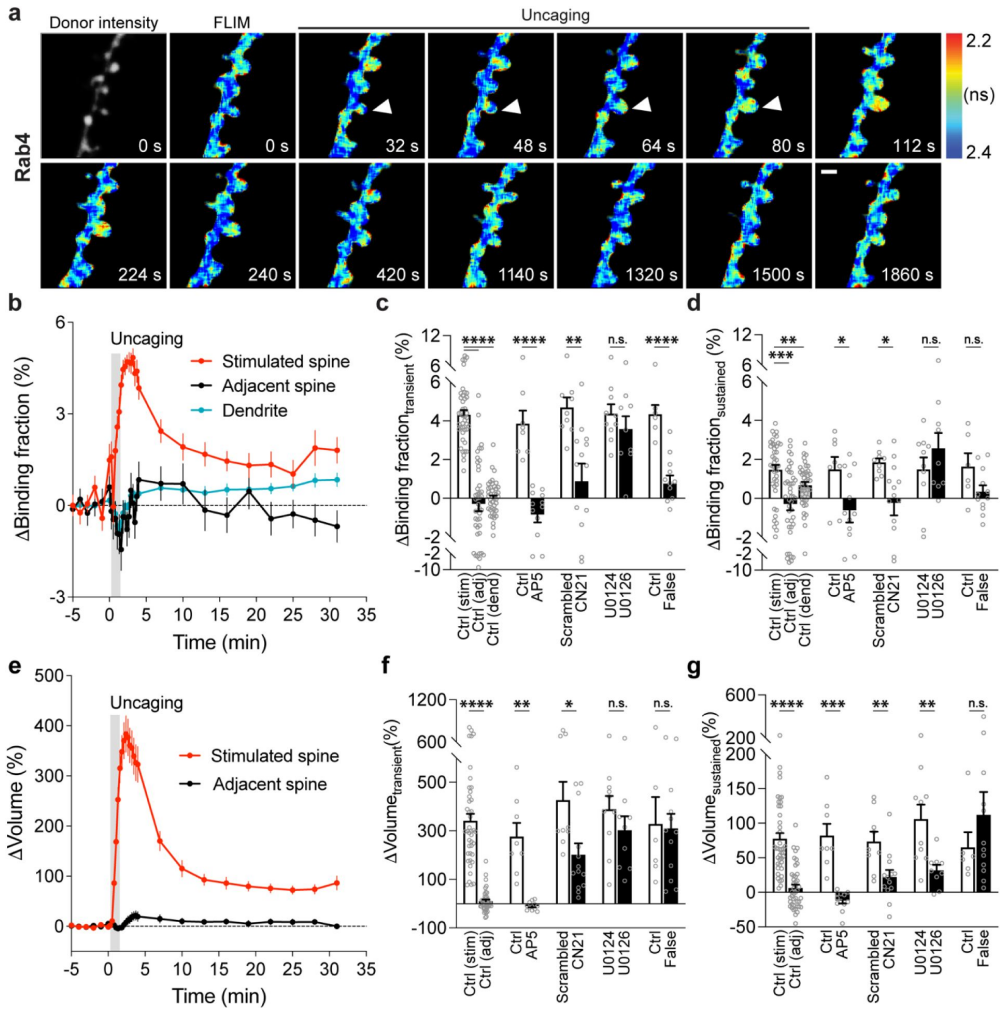

Fig. 3

Spatiotemporal dynamics of Rab4 activation during sLTP induced at single spines.

a, Representative donor fluorescence intensity image (gray) and fluorescence lifetime (FLIM, colorful) images of Rab4 activation during sLTP induced by two-photon glutamate uncaging. Arrowheads indicate the stimulated spine. The warmer color indicates shorter lifetime and higher Rab4 activity. Scale bar represents 1 μm. **b**, Averaged time courses of Rab4 activation measured as binding fraction changes between mEGFP-Rab4 and mCherry-Rabenosyn5 [439-503]-mCherry in the stimulated spine (red), adjacent spine (black) and dendrite (blue). Grey rectangle bar indicates glutamate uncaging (0.5 Hz, 60 s). Data are presented in mean ± SEM. N=42/34 (spine/neuron), 42/34 (spine/neuron), and 42/34 (dendrite/neuron) for the stimulated spine, adjacent spine and dendrite, respectively. **c,d**, Quantification of Rab4 binding fraction changes in the transient phase (c, averaged over 1.3-4 min) and sustained phase (d, averaged over 19-31 min) in the stimulated spine (stim), adjacent spine (adj) and dendrite (dend) for the same experiments as b. Data represent mean ± SEM. One-way ANOVA followed by Bonferroni's multiple comparison tests were used for the stimulated spine, adjacent spine and dendrite (** p<0.01, *** p<0.001, **** p<0.0001). Effects of pharmacological agents on Rab4 activation in the stimulated spines are also presented. All pharmacological inhibition experiments were paired with controls from the same batch of slices. Data represent mean ± SEM. Student's t-tests were performed (n.s., not significant, * p<0.05, ** p<0.01, **** p<0.0001). N=8/6, 12/9, 9/8, 13/11, 10/8 and 9/8 (spine/neuron) for Ctrl, AP5, scrambled, CN21, U0124 and U0126, respectively. When mEGFP-Rab4 was paired with a false acceptor (False), mCherry-Rim1 [20-227]-mCherry, little activity change was observed in the stimulated spines. Data represent mean ± SEM. Student's t-tests were performed (n.s., not significant, **** p<0.0001). N=6/5 and 12/9 (spine/neuron) for Ctrl and False, respectively. **e**, Averaged time courses of spine volume change in the same experiments as b. Data represent mean ± SEM. **f,g**, Quantification of spine volume changes in the transient phase (f, averaged over 1.3-4 min) and sustained phase (g, averaged over 19-31 min) for the same experiments as c and d. Data represent mean ± SEM. Student's t-tests were used for all groups (n.s., not significant, * p<0.05, ** p<0.01, *** p<0.001, **** p<0.0001).

Disruption of Rab10 signaling enhances structural and electrophysiological LTP, whereas disruption of Rab4 signaling inhibits the transient phase of structural LTP

Given that Rab10 and Rab4 display opposing activity profiles during sLTP, we hypothesized that they would have opposite functions in spine structural plasticity. To test this hypothesis, we knocked down Rab10 or Rab4 by respective shRNA, and examined the effects of these manipulations on sLTP. We biolistically transfected cultured organotypic hippocampal slices of rats with scrambled shRNA control or shRNA against Rab10 or Rab4, together with mEGFP as the volume marker. Compared with scrambled shRNA control, knockdown of Rab10 had no effect on spine size, but increased spine density (**Fig. 4a** and **Extended Data Fig. 11a,b,f,g,h,i**). Knockdown of Rab4 had no effect on spine size or density (**Fig. 4a** and **Extended Data Fig. 11a,b,e,g,h,i**).

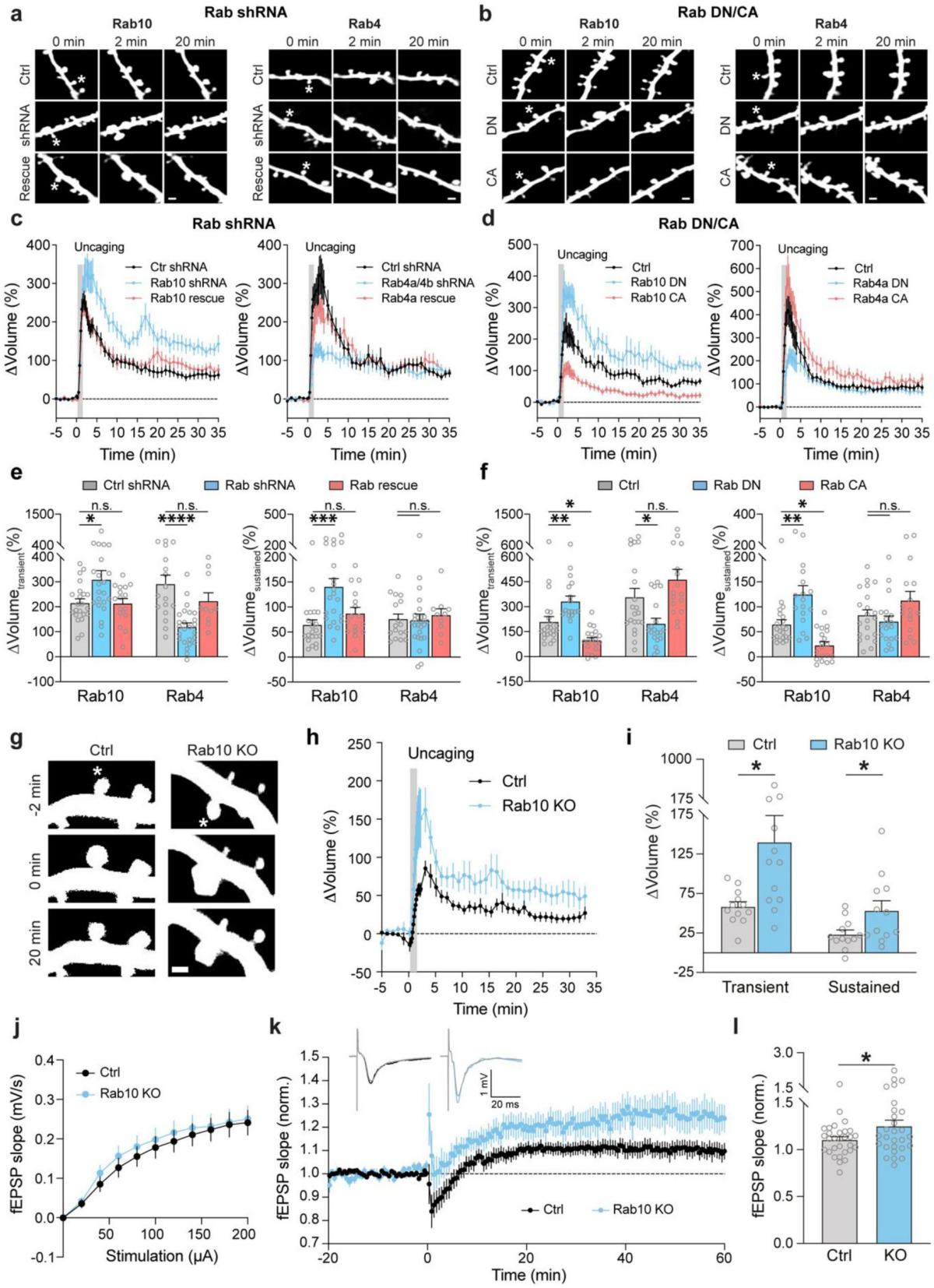
a
Rab shRNA
Rab10
Rab4
0 min
2 min
20 min
Ctrl
shRNA
Rescue
b
Rab DN/CA
DN
CA
c
Uncaging
Ctr shRNA
Rab10 shRNA
Rab10 rescue
Ctrl shRNA
Rab4a/4b shRNA
Rab4a rescue
ΔVolume (%)
Time (min)
d
Ctrl
Rab10 DN
Rab10 CA
Rab4a DN
Rab4a CA
e
Ctrl shRNA
Rab shRNA
Rab rescue
n.s.
Rab10
Rab4
f
Ctrl
Rab DN
Rab CA
g
Ctrl
Rab10 KO
-2 min
0 min
20 min
h
i
Transient
Sustained
j
fEPSP slope (mV/s)
Stimulation (μA)
k
fEPSP slope (norm.)
1 mV
20 ms
l
Ctrl
KO

Fig. 4

Rab4 positively regulates transient phase of structural LTP and Rab10 negatively regulates structural and electrophysiological LTP.

a,b, Representative fluorescence images of spine volume change in the stimulated spines after manipulations of Rab10 and Rab4 signaling. Asterisks indicate the stimulated spines. Scale bars represent 1 μm. **a,** Left: rat CA1 pyramidal neurons were transfected with mEGFP and scrambled shRNA (Ctrl shRNA); mEGFP and shRNA against Rab10 (Rab10 shRNA); mEGFP, shRNA against Rab10, and mCherry-shRNA-resistant Rab10 (Rab10 rescue). Right: rat CA1 pyramidal neurons were transfected with mEGFP and scrambled shRNA (Ctrl shRNA); mEGFP and shRNAs against Rab4a and Rab4b (Rab4a/4b shRNA); mEGFP, shRNAs against Rab4a and Rab4b, and mCherry-shRNA-resistant Rab4a (Rab4a rescue). **b**, Left: rat CA1 pyramidal neurons were transfected with mEGFP (Ctrl); mEGFP and mCherry-Rab10 [T23N] (Rab10 DN); mEGFP and mCherry-Rab10 [Q68L] (Rab10 CA). Right: rat CA1 pyramidal neurons were transfected with mEGFP (Ctrl); mEGFP and mCherry-Rab4a [S27N] (Rab4a DN); mEGFP and mCherry-Rab4a [Q72L] (Rab4a CA). **c,d,** Averaged time course of spine volume change for experiments in a and b. Fluorescence intensity of mEGFP was used to measure the spine volume change. Data represent means ± SEM. All experiments were paired with the same day controls from the same batch of slices. **c**, Left: N=22/20, 22/20 and 16/13 (spine/neuron) for Ctrl shRNA (black), Rab10 shRNA (blue) and Rab10 rescue (red), respectively. Right: N=17/17, 25/21 and 10/8 (spine/neuron) for Ctrl shRNA (black), Rab4a/4b shRNA (blue) and Rab4a rescue (red), respectively. **d,** Left: N=22/18, 17/15 and 19/14 (spine/neuron) for Ctrl (black), Rab10 DN (blue) and Rab10 CA (red), respectively. Right: N=21/15, 19/18 and 16/11 (spine/neuron) for Ctrl (black), Rab4a DN (blue) and Rab4a CA (red), respectively. **e,f**, Quantitative analysis of the transient volume change (volume change averaged over 1.3-4 min, left) and the sustained volume change (volume change averaged over 20-35 min, right) for c in e and for d in f. Data represent means ± SEM. One-way ANOVA followed by Bonferroni's multiple comparison tests were performed (n.s., not significant, * p<0.05, ** p<0.01, *** p<0.001, **** p<0.0001). **g,** Representative fluorescence images of stimulated spine volume change in CA1 pyramidal neurons from *Rab10*$^{fl/fl}$ mice transfected with tdTomato-Cre and mEGFP (Rab10 KO), or tdTomato and mEGFP as a control (Ctrl). Asterisks indicate the stimulated spines. Scale bars represent 1 μm. **h**, Averaged time courses of stimulated spine volume change for experiments in g. Data represent means ± SEM. N=12 for Ctrl (black) and 12 for Rab10 KO (blue). **i**, Quantification of the transient volume change (left) and the sustained volume change (right) for h. Data represent means ± SEM. Unpaired two-tailed Student's t-tests were used (* p<0.05). **j**, Electrophysiological recordings showing average input/output curve of *Rab10*$^{fl/fl}$:*CaMKIIα-Cre*$^{+/-}$ mice (Rab10 KO, blue, n=11) and littermate *Rab10*$^{fl/fl}$:*CaMKIIα-Cre*$^{-/-}$ control mice (Ctrl, black, n=11). Data are mean ± SEM. **k**, Time course of extracellularly recorded excitatory postsynaptic potential (fEPSP) slope before and after LTP induction in CA1 pyramidal neurons from *Rab10*$^{fl/fl}$:*CaMKIIα-Cre*$^{+/-}$ mice (blue, number of slices/animals = 28/7) and littermate *Rab10*$^{fl/fl}$:*CaMKIIα-Cre*$^{-/-}$ mice (black, n = 30/8). Data are represented as mean ± SEM. Insets (top) are the representative traces of fEPSP before and after stimulation for Cre+ (blue) and Cre-(black) mice. **l**, Quantification of the average fEPSP slope at 40-60 min for experiments in k. Data are mean ± SEM. Unpaired two-tailed Student's t-tests were used (* p<0.05).

We further induced sLTP by two-photon glutamate uncaging in single spines of neurons expressing mEGFP[6,62]. Under control condition with scrambled shRNA, application of a train of glutamate uncaging pulses (0.5 Hz, 60 s) in zero extracellular Mg^{2+} induced a rapid spine volume increase in the transient phase, which decayed to a sustained enlarged volume for more than 30 min (**Fig. 4a,c**). However, knockdown of Rab10 by shRNA enhanced spine enlargement both in the transient and sustained phase of sLTP, which was rescued by co-expressing shRNA-resistant Rab10 (for scrambled shRNA, $\Delta V_{transient}$ = 215.5 ± 16.6% and $\Delta V_{sustained}$ = 64.4 ± 9.9%; for Rab10 shRNA, $\Delta V_{transient}$ = 309.0 ± 36.3% and $\Delta V_{sustained}$ = 140.6 ± 16.4%; for Rab10 rescue, $\Delta V_{transient}$ = 213.5 ± 19.7% and $\Delta V_{sustained}$ = 87.4 ± 11.7%; **Fig. 4a,c,e** and **Extended Data Fig. 11a,b,d,f,g**). In contrast, knockdown of Rab4 by shRNA significantly impaired the transient phase of sLTP while leaving the sustained phase intact (for scrambled shRNA, $\Delta V_{transient}$ = 291.6 ± 35.6% and $\Delta V_{sustained}$ = 76.1 ± 10.0%; for Rab4a/4b shRNA, $\Delta V_{transient}$ = 119.8 ± 15.4% and $\Delta V_{sustained}$ = 73.8 ± 12.1%; **Fig. 4a,c,e** and **Extended Data Fig. 11a,b,e,g**). This phenotype was

rescued by coexpression of shRNA-resistant Rab4a ($\Delta V_{transient}$ = 223.1 ± 32.8% and $\Delta V_{sustained}$ = 84.2 ± 12.3%; **Fig. 4a,c,e** and **Extended Data Fig. 11c**). Overall, these results suggest that Rab10 negatively regulates both the transient and sustained phases of sLTP, while Rab4 is required for the transient phase of sLTP.

As an alternative strategy to inhibit Rab10 and Rab4 functions, we examined the effects of overexpressing DN-Rab mutants on spine structural plasticity. Consistent with the shRNA results, DN-Rab10 enhanced both the transient and sustained phase of sLTP (for control, $\Delta V_{transient}$ = 209.2 ± 31.1% and $\Delta V_{sustained}$ = 64.8 ± 9.4%; for Rab10 DN, $\Delta V_{transient}$ = 332.0 ± 31.8% and $\Delta V_{sustained}$ = 125.0 ± 17.4%; **Fig. 4b,d,f**) , while DN-Rab4a selectively inhibited the transient phase of sLTP (for control, $\Delta V_{transient}$ = 357.4 ± 52.0% and $\Delta V_{sustained}$ = 83.5 ± 10.8%; for Rab4a DN, $\Delta V_{transient}$ = 198.1 ± 32.1% and $\Delta V_{sustained}$ = 70.8 ± 11.0%; **Fig. 4b,d,f**). Moreover, we evaluated the effect of overexpressing CA-Rab10 or CA-Rab4 on sLTP. These manipulations in general caused opposite phenotypes to the DN mutants: CA-Rab10 decreased both the transient and sustained phase of sLTP (for control, $\Delta V_{transient}$ = 209.2 ± 31.1% and $\Delta V_{sustained}$ = 64.8 ± 9.4%; for Rab10 CA, $\Delta V_{transient}$ = 97.7± 16.5% and $\Delta V_{sustained}$ = 23.0 ± 7.1%; **Fig. 4b,d,f**), while CA-Rab4 slightly increased the transient phase of sLTP (but not statistically significant; for control, $\Delta V_{transient}$ = 357.4 ± 52.0% and $\Delta V_{sustained}$ = 83.5 ± 10.8%; for Rab4a CA, $\Delta V_{transient}$ = 463.1 ± 61.1% and $\Delta V_{sustained}$ = 112.7 ± 18.3%; **Fig. 4b,d,f**).

We further evaluated the effects of Rab10 deletion on structural and electrophysiological LTP using Rab10 conditional knockout mice ($Rab10^{fl/fl}$)[63]. For sLTP measurement, we biolistically transfected cultured organotypic hippocampal slices of $Rab10^{fl/fl}$ mice with tdTomato-fused Cre recombinase and mEGFP, or tdTomato and mEGFP as a control[64]. Consistent with the Rab10-knockdown results, deletion of the *Rab10* gene increased sLTP in the stimulated spines of CA1 pyramidal neurons (**Fig. 4g,h,i**). Furthermore, we crossed $Rab10^{fl/fl}$ mice with *Camk2a-Cre* mice ($Rab10^{fl/fl}$:$Camk2a\text{-}Cre^{+/-}$) to postnatally remove Rab10 from forebrain excitatory neurons[65]. These animals showed enhanced

LTP upon theta burst stimulation (TBS) at Schaeffer collateral synapses (**Fig. 4k,l**), with the basal synaptic transmission unchanged (**Fig. 4j**). Moreover, we monitored Schaffer collateral synaptic transmission in these mice, and found no difference in the amplitude of AMPAR- and NMDAR-EPSCs, or AMPAR/NMDAR EPSC ratio (**Extended Data Fig. 12**). These results indicate that Rab10 is a negative regulator for electrophysiological LTP.

Overall, our results demonstrate that Rab10 negatively regulates both the transient and sustained phase of sLTP, while Rab4 positively regulates the transient phase of sLTP. These functions are consistent with the direction and time window of their activity changes during sLTP. Moreover, Rab10 negatively modulates electrophysiological LTP.

Rab10 and Rab4 oppositely regulate activity-dependent SEP-GluA1 exocytosis during sLTP

We further examined whether Rab10 and Rab4 play roles in the exocytosis of GluA1-containing vesicles during sLTP[66]. To visualize newly exocytosed AMPARs from the intracellular compartments during sLTP, we combined fluorescence recovery after photobleaching (FRAP) with two-photon glutamate uncaging and two-photon imaging[66,67]. Organotypic hippocampal slices were biolistically transfected with N-terminal super-ecliptic pHluorin (SEP)-tagged GluA1, mCherry, and scrambled shRNA. CA1 pyramidal neurons expressing mCherry and SEP-GluA1 were imaged under two-photon microscopy. Since SEP-GluA1 is quenched in the acidic environment of endosomes, only the population on the surface emits fluorescence[66–68].

We pre-bleached surface SEP-GluA1 in a whole secondary dendrite with two-photon excitation, and measured the fluorescence recovery due to exocytosis in the spines after the induction of sLTP. Upon glutamate uncaging, the volume of the stimulated spines, measured with mCherry fluorescence, was increased by 352.8 ± 34.3% at 2 min (**Fig. 5a,b**). Meanwhile, the fluorescence intensity of SEP-GluA1 was rapidly recovered from 15.4 ± 1.6% (0 min) to 108.8 ± 10.8% (2 min) in the stimulated spines (**Fig. 5a,b**). However, in the non-stimulated adjacent spines and dendrites, SEP-GluA1 recovery was smaller and slower (for adjacent spines, from 17.3 ± 1.3% at 0 min to 28.9 ± 2.7% at 2 min; for dendrites, from 27.8 ± 1.4% at 0 min to 43.9 ± 1.9% at 2 min; **Fig. 5a,b**). Overexpression of tetanus toxin light chain (TeTxLC), which cleaves vesicle-associated membrane protein (VAMP)[69], significantly decreased both the spine enlargement and the SEP-GluA1 recovery in the stimulated spines, suggesting that the fluorescence recovery requires exocytosis (**Fig. 5c-f** and **Extended Data Fig. 13a**).

To investigate whether Rab10 and Rab4 are involved in this activity-dependent postsynaptic AMPAR exocytosis, we knocked down endogenous Rab10 or Rab4 by respective shRNA, and monitored SEP-GluA1 exocytosis and sLTP in the stimulated and adjacent spines. No significant difference was seen in the adjacent spines or dendrites in either SEP-GluA1 recovery or mCherry intensity change among all groups (**Extended Data Fig. 14a-h**). Compared with scrambled shRNA, expression of Rab10 shRNA enhanced the spine enlargement as well as SEP-GluA1 incorporation (**Fig. 5a,c**-f and **Extended Data Fig. 13d**; measured at 2 min). These phenotypes were rescued by coexpressing shRNA-resistant Rab10 (**Fig. 5a,c**-f and **Extended Data Fig. 13e**; measured at 2 min). Therefore, Rab10 negatively regulates GluA1 exocytosis in the stimulated spines during sLTP. In contrast, the expression of Rab4a and Rab4b shRNAs impaired spine enlargement (**Fig. 5a,e,f** and **Extended Data Fig. 13b**; measured at 2 min). It also significantly attenuated SEP-GluA1 recovery in the stimulated spines (**Fig. 5a,c,d** and **Extended Data Fig. 13b**; measured at 2 min). These phenotypes were rescued by coexpressing shRNA-resistant Rab4a (**Fig. 5a,c**-f and **Extended Data Fig. 13c**; measured at 2 min). These findings suggest that Rab4 is required for GluA1 exocytosis in the stimulated spines during sLTP. Moreover, compensating for the effect of SEP-GluA1's lateral diffusion by subtracting the change in the spine surface area (ΔVolume [2]/[3]) (**Extended Data Fig. 14i**)[66] did not alter our findings. Therefore, during sLTP Rab10 limits and Rab4 enhances SEP-GluA1 incorporation in the stimulated spines.

Discussion

The development of novel FRET-based biosensors for Rab proteins has revealed how Rab signaling pathways regulate sLTP in single dendritic spines. In brief, NMDAR activation triggers Ca^{2+} influx (~ms) and CaMKII activation (~s)[62,70], leading to the persistent inactivation of Rab10 (~min) and transient activation of Rab4 (~min) (**Fig. 5g**). Consistent with the directions and the duration of their activity change, Rab10 negatively regulates both the transient and sustained phase of sLTP and electrophysiological LTP. In contrast, Rab4 positively regulates the transient phase of sLTP. Thus, the temporal dynamics of Rab10 and Rab4 mirror the time courses of their functions in sLTP. Furthermore, Rab10 inhibits activity-dependent AMPAR trafficking during sLTP, while Rab4 promotes this process (**Fig. 5g**). These results suggest that Rab4 and Rab10 play critical roles in two membrane trafficking events – AMPAR trafficking and spine enlargement – during sLTP.

Understanding the kinetics of Rab4 and Rab10 sensors is essential for interpreting their actual activity during sLTP. The Rab4 sensor exhibits a rapid rise and fall in activation (**Fig. 3**), indicating ON/OFF times of less than a few minutes. In contrast, the Rab10 sensor rapidly dissociates during sLTP induction (**Fig. 2**), with OFF kinetics occurring within one minute and fast ON kinetics in response to NMDA (**Fig. 1j**). Given these rapid kinetics, the observed sustained inactivation of Rab10 likely reflects its true behavior rather than sensor dynamics.

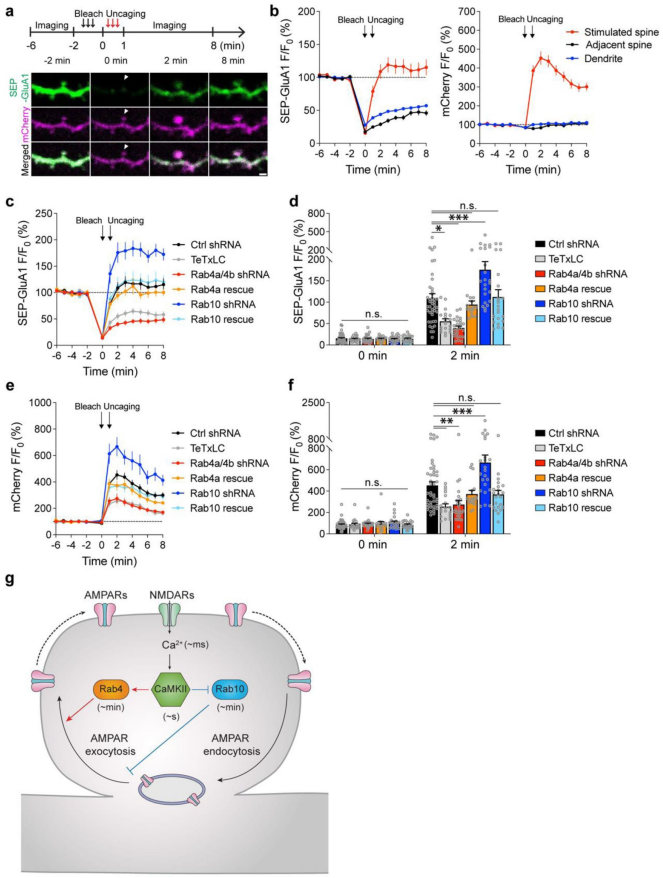

Fig. 5

Rab4 and Rab10 positively and negatively regulate activity-dependent SEP-GluA1 exocytosis in the stimulated spines during sLTP, respectively.

a, Upper panel: schematic for SEP-GluA1 FRAP and two-photon glutamate uncaging experiment. Whole dendrite photobleaching was performed from -2 min to 0 min, followed by single spine glutamate uncaging from 0 min to 1 min (0.5 Hz, 60 s). Lower panel: representative pseudo color images of SEP-GluA1 (green) FRAP after two-photon glutamate uncaging in a single spine of hippocampal CA1 pyramidal neurons coexpressing mCherry (magenta) and scrambled shRNA. White arrowheads indicated the stimulated spine. Scale bar represents 1 μm. **b**, Averaged time courses of SEP-GluA1 (left) and mCherry (right) fluorescence intensity (F/F_0) in the stimulated spine (red), adjacent spine (black) and dendrite (blue) of neurons expressing SEP-GluA1, mCherry, and scrambled shRNA. Black arrows indicate the time points after photobleaching and glutamate uncaging, respectively. Data represent mean ± SEM. N=43/35 (spine/neuron), 43/35 (spine/neuron) and 43/35 (dendrite/neuron) for the stimulated spine, adjacent spine and dendrite, respectively. **c**, Averaged time courses of SEP-GluA1 FRAP in the stimulated spines of neurons expressing SEP-GluA1, mCherry, and scrambled shRNA (Ctrl shRNA, black, n=43/35); SEP-GluA1, mCherry, and TeTxLC (TeTxLC, grey, n=19/12); SEP-GluA1, mCherry, and shRNAs against Rab4a and Rab4b (Rab4a/4b shRNA, red, n=26/16); SEP-GluA1, mCherry, shRNAs against Rab4a and Rab4b, and shRNA-resistant Rab4a (Rab4a rescue, orange, n=16/12); SEP-GluA1, mCherry, and shRNA against Rab10 (Rab10 shRNA, green, n=23/15); SEP-GluA1, mCherry, shRNA against Rab10, and shRNA-resistant Rab10 (Rab10 rescue, blue, n=22/19). Data represent mean ± SEM. All experiments were paired with the same day controls from the same batch of slices. **d**, Quantification of SEP-GluA1 fluorescence intensity at 0 min and 2 min in the same experiments as c. Data represent mean ± SEM. One-way ANOVA followed by Bonferroni's multiple comparison tests were performed (n.s., not significant, * p<0.05, *** p<0.001). **e**, Averaged time courses of mCherry fluorescence intensity in the stimulated spines of the same neurons as c. Data represent mean ± SEM. **f**, Quantification of mCherry fluorescence intensity at 0 min and 2 min in the same experiments as c. Data represent mean ± SEM. One-way ANOVA followed by Bonferroni's multiple comparison tests (n.s., not significant, ** p<0.01, *** p<0.001). Please note that the Ctrl shRNA samples in c-f are the same as those in a-b. **g**, Proposed model for Rab4 and Rab10 mediated AMPAR trafficking and sLTP. Activation of postsynaptic NMDARs triggers Ca^{2+} influx (~ms) and CaMKII activation (~s), which is relayed by the transient activation of Rab4 (~min) and persistent inactivation of Rab10 (~min). Rab4 activation and Rab10 inactivation result in the potentiated AMPAR exocytosis and sLTP induction in single dendritic spines.

Previous studies have suggested that gating of signaling regulates kinase-phosphatase balance during LTP. For example, activation of the cyclic adenosine monophosphate (cAMP) pathway inactivates protein phosphatase, thereby gating CaMKII signaling[71–73]. Here we demonstrated that Rab10 is inactivated during sLTP and plays inhibitory roles in AMPAR trafficking and spine enlargement, suggesting that Rab10 acts as a gate for the membrane trafficking events during sLTP. Thus, gating of inhibitory signaling is likely a common mechanism in synaptic plasticity.

On the other hand, Rab4 facilitates membrane expansion and AMPAR trafficking, specifically during the transient phase of sLTP. In a previous study, LTP onset appears to be delayed in Rab4 knock-down neurons, implicating that Rab4 is required for the rapid increase of AMPAR current during LTP induction[30]. Indeed, Rab4 is rapidly recruited into the spines in the transient phase of sLTP (**Extended Data Fig. 6d-f**). Consistently, recent ultrastructural analyses also demonstrated the increase of PSD complexity and membrane expansion during the transient phase of sLTP[7]. RhoA is another signaling molecule that plays a role specifically in the transient phase, likely by organizing the actin cytoskeleton in spines[6]. These signaling processes to rapidly reorganize spine structure during the transient phases would be critical for shaping the onset of synaptic transmission during LTP and sLTP.

Interestingly, Rab4, 5, 7, 8 and 10 sensors are all activated upon low-dose NMDA application (**Fig. 1j** and **Extended Data Fig. 1e**). However, they displayed distinct time courses and durations of activity change (**Fig. 1j** and **Extended Data Fig. 1e**). It is known that bath application of low-concentration NMDA induces LTD and dephosphorylation of AMPARs in the hippocampus[80]. During LTD, the rate of AMPAR internalization outweighs the rate of AMPAR exocytosis, resulting in a reduced number of synaptic AMPARs. Since Rab proteins are localized on different endosomes and coordinate individual parts of receptor trafficking, their distinct time courses and activity durations may reflect the involvement of related endosomes in LTD. Particularly, Rab10 sensor displayed bi-directional activity changes in response to sLTP or chemical LTD induction. To fully understand Rab10's function in synaptic plasticity, it would be necessary to investigate its involvement in LTD.

Notably, the inactivation of Rab10 is persistent and lasts for over 30 min. Despite different time courses of activity during sLTP, other small GTPases RhoA, Cdc42, Rac1 and Ras also remain activated over 20 min[6,57,58]. Moreover, BDNF-TrkB signaling is rapidly activated in the spines and remains elevated for at least 60 min during sLTP[13]. The persistent inactivation pattern of Rab10 is possibly defined by the activity of its associated endosomal organelle in sLTP. Previous studies showed that Rab10 is localized on various membranes, including the early endosome, recycling endosome, endoplasmic reticulum (ER), Golgi and trans-Golgi network (TGN). With SLENDR-mediated knockin technique, we found that endogenous Rab10 is majorly overlapped with Rab7-labelled lysosome, partially colocalized with Rab11-labelled recycling endosome, but separated from Rab5-labelled early endosome *in vivo* (**Extended Data Fig. 1j**). These results implicate that Rab10 may mediate the transport from recycling endosome to lysosome for protein degradation. Therefore, inactivation of Rab10 possibly inhibits AMPAR degradation pathway, resulting in more available AMPARs for synaptic insertion and synaptic potentiation.

Pharmacological analysis of Rab10 and Rab4 signaling pathways indicated that they are downstream of CaMKII, but not ERK. Previously, the Ras-ERK pathway has been implicated in regulating AMPAR delivery and sLTP[58,66,74]. Our data suggest that Rab10 and Rab4 act as parallel pathways that are independent of Ras-ERK signaling. The steps between CaMKII activation and Rab10 inactivation or Rab4 activation are still unclear. One possibility is through the direct phosphorylation of Rab proteins[75,76], or indirect regulations by Rab GAPs or GEFs. Interestingly, in contrast to the Ras-ERK pathway, which shows extensive spreading into dendrites or nucleus[58,77,78], the activity of Rab10 and Rab4 is restricted to the stimulated spines during sLTP. Thus, Rab10 and Rab4 may regulate local membrane trafficking in spines, whereas

ERK may regulate AMPAR exocytosis in dendrites[66], through different downstream effectors. Notably, a spine-restricted pattern of signaling activity has also been observed for Cdc42 and Cofilin activation during sLTP, which promotes the actin polymerization[6,79]. Given that some Rab proteins are known to regulate actin polymerization[91], it is plausible that they influence AMPAR exocytosis and spine enlargement through modulation of actin dynamics. Thus, the combination of local membrane trafficking and actin polymerization in spines appears important for spine expansion during sLTP.

Finally, our results highlight the diverse roles of Rab proteins in the orchestrated regulation of membrane trafficking during sLTP. It appears that Rab proteins operate in different directions and time windows. Whereas Rab10 negatively regulates sLTP for a long time (~30 min), Rab4 positively regulates the initial ~5 min of sLTP. Coordination of the upregulation and downregulation of the activity of various Rab proteins with unique functional and temporal properties would allow for the flexible and reliable control of membrane trafficking in multiple forms of spine structural plasticity. Although we measured the activity of only two Rab proteins in sLTP, it is likely that other members among the ~60 Rab family proteins are critical for different spatiotemporal aspects of spine structural plasticity. Imaging the activity of other Rab proteins using similar Rab sensors will hopefully reveal the coordinated signaling that regulates membrane trafficking during synaptic plasticity.

Methods

HEK 293T cells

HEK 293T cell lines were obtained from Fisher Scientific (Cat# NC0260915), and grown in DMEM (Gibco) supplemented with 10% fetal bovine serum (Invitrogen) and 1% penicillin-streptomycin (Invitrogen). The cell cultures were maintained at 37°C in a 5% CO_2 humidified atmosphere.

Rat

CD wild-type rats (CD IGS) purchased from Charles River Laboratories were used for preparation of hippocampal organotypic slice culture and dissociated postnatal cortical neuron culture. Both male and female animals were used and randomly allocated to experimental groups. All the experiments were performed in accordance with guidelines from the US National Institutes of Health, and were approved by Duke University Medical Center and the Institutional Animal Care and Use Committee of Max Planck Florida Institute for Neuroscience.

Mice

Rab10 conditional knockout (*Rab10*$^{fl/fl}$) mouse was a gift from Dr. Timothy E McGraw[63]. *Camk2a-Cre* mouse was as previously[65]. Swiss Webster mice were obtained from Charles River for endogenous Rab10 knockin experiments. Both of male and female mice were used. All the experiments were performed in accordance with guidelines from the US National Institutes of Health, and were approved by the Institutional Animal Care and User Committee of Max Planck Florida Institute for Neuroscience.

Organotypic slice culture

Organotypic rat or mouse hippocampal slices were prepared at postnatal day 6 or 7, as previously described[81]. Briefly, coronal hippocampal slices were dissected at 400 µm thickness using a McIlwain tissue chopper (Ted Pella, Inc). The slices were cultured on hydrophilic PTFE membranes (Millicell, Millipore), which were inserted in the culture medium containing 8.4 mg/ml MEM

(Sigma), 20% horse serum (Gibco), 1 mM L-Glutamine (Sigma), 5.2 mM $NaHCO_3$, 12.9 mM D-Glucose, 0.075% Ascorbic acid, 30 mM Hepes,1 µg/ml Insulin, 1 mM $CaCl_2$ and 2 mM $MgSO_4$. The slice cultures were maintained at 35°C in a 5% CO_2 humidified atmosphere.

Dissociated neuron culture

Dissociated postnatal cortical cultures were prepared as previously published[82]. Briefly, cortices dissected from newborn rats (ramdom male and female) were triturated and plated into 5 cm dishes coated with 50 µg/ml PLL (Sigma) in culture medium consisting of Basal Medium Eagle (BME) supplemented with 10% heat-inactivated fetal bovine serum (Invitrogen), 35 mM glucose (Sigma), 1 mM L-glutamine (Sigma), 100 U/ml penicillin (Sigma), and 0.1 mg/ml streptomycin (Sigma). Neuron cultures were maintained at 35°C in a 5% CO_2 humidified atmosphere.

DNA constructs

To generate pCAGGS-mCherry, pCAGGS-mTurquoise2, pCAGGS-mCherry-mCherry, and pCAGGS-mVenus-mVenus, the respective fluorescence protein sequence was cloned into pCAGGS backbone from Raichu-2517KX gifted from Dr. Michiyuki Matsuda[83]. Rat full length Rab4a, Rab5a, Rab7a, Rab8a, Rab11a and Rab10 were amplified by PCR from rat brain cDNA library (Dharmacon, Cat# LRN1205) and cloned into pmEGFP-C1[6], pCAGGS-mEGFP, pCAGGS-mCherry and pCAGGS-mTurquoise2. All FRET donors were tagged at the amino terminus of Rab proteins. The linker between FRET donors (mEGFP or m Turquoise2) and Rab GTPases is SGLRSRG. Rabenosyn5 [439-503], EEA1[36-128], FYCO1[963-206], Rim2 [27-175] and Rim1 [20-227] cDNAs were amplified by PCR from rat brain cDNA library and inserted into pCAGGS-mCherry-mCherry and pCAGGS-mVenus-mVenus constructs. The linkers between mCherry and RBDs is SGLRSRA for the amino terminus and GSG for the carboxy terminus. The linkers between mVenus and Rim1 [20-227] is SGLRSRG for the amino terminus and GSG for the carboxy terminus. Rab dominant negative (DN) and constitutively active (CA) mutants were generated from wild type Rab GTPases by site-directed mutagenesis, and subcloned into pCAGGS-mEGFP, pCAGGS-3Flag and pCAGGS-mCherry constructs. PIK3R1 [114-313], Rin1, RNTre, RabGAP5, GRAB, Rabin8, TBC1D10 was amplified from rat brain cDNA library and cloned into pCAGGS-3HA construct. Full length Dennd4c, Evi5 and Rab3gap1 were amplified by PCR from MGC mouse cDNA (Dharmacon) and subcloned into pCAGGS-3HA construct. psiCHECK-2-Sal4-wt_3'UTR was a gift from Robert Blelloch (Addgene plasmid # 31862). psiCHECK-2-Rab GTPases were generated by inserting Rab GTPases into psiCHECK-2-Sal4-wt_3'UTR by XhoI/NotI.Tetanus toxin light chain[84] was subcloned into pCAGGS-3Flag construct. SEP-GluA1 was a gift from Dr. Scott Soderling at Duke University[23]. mTurquoise2-pBAD and mVenus-pBAD were gifts from Michael Davidson (Addgene plasmid # 54844 and # 54845). The human codon-optimized S. pyogenes Cas9 (SpCas9) and single guide RNA (sgRNA) expression plasmid was a gift from F. Zhang (pX330, Addgene plasmid # 42230)[85].

RNA interference

For shRNA-mediated knock-down of Rab4 and Rab10, we used SHCLND-NM_009003 plasmid for Rab4a (Sigma-Aldrich, TRCN0000088975), SHCLND-NM_016154 palsmid for Rab4b (Sigma-Aldrich, TRCN0000380038), and TRC-Mm1.0 plasmid for Rab10 (Dharmacon, TRCN0000100838). The respective shRNA sequences (according to manufacture and sequencing confirmation) are CCGGAGATGACTCAAATCATACCATC TCGAGATGGTATGATTTGAGTCATCTTTTTTG for Rab4a, GTACCGGGGTCATCCTC TGTGGCAACAACTCGAGTTGTTGCCACAGAGGATGACCTTTTTTG for Rab4b, and T TGCCTTTCGGTACAACTCTC (mature antisense) for Rab10. For shRNA control, we used scrambled shRNA with the following sequence: CCTAAGGTTAAGTCGCCCTCG CTCGAGCGAGGGCGACTTAACCTTAGG (Addgene plasmid # 1864). To visualize transfected neurons in sLTP experiments, mEGFP was inserted into scrambled shRNA, Rab4a and Rab10 shRNA by KpnI/BamHI, and into Rab4b shRNA by BamHI/BstEII. The mEGFP expression was driven by a separate hPGK promoter (shRNA/mEGFP). For the rescue experiments, silent mutations of three

amino acids were induced at the targeted region for Rab4a and Rab10 by site-directed mutagenesis (for shRNA-resistant Rab4a, AAAGATGACTC**C**AA**C**CA**C**ACCATA; for shRNA-resistant Rab10, GAGAGTTGT**G**CC**C**AA**G**GGCAA).

Transfection of FRET sensors in HEK 293T cells and organotypic slice cultures

HEK 293T cells were transfected with Lipofectamine 2000 following the manufacture's recommendations (Invitrogen), and imaged 24-48 hours after transfection. For Rab GTPase FRET sensors, the ratio of transfected FRET donor and acceptor was 1:3.

After 9-13 days in culture, organotypic hippocampal slices were transfected biolistically with gene gun[86] (Bio-Rad, pressure 200 psi) using gold beads (Bio-Rad, 1.6 μm) coated with plasmids, and imaged 3-4 days after transfection. For Rab4 FRET sensor, pmEGFP-Rab4a and pCAGGS-mCherry-Rabenosyn5 [439-503]-mCherry (1:1, 20 μg) were expressed for 3 days. For Rab10 FRET sensor, pCAGGS-mTurquoise2-Rab10 and pCAGGS-mVenus-Rim1 [20-227]-mVenus (1:3, 40-60 μg) were expressed for 3-4 days.

Two-photon fluorescence lifetime imaging and two-photon glutamate uncaging

We used a custom-built two-photon fluorescence lifetime imaging microscope (2pFLIM) with two Ti:Sapphire lasers (Chameleon, Coherent) as previously described[42,87]. One laser was tuned to 920 nm to excite both donor for lifetime measurement and acceptor for morphology. The second laser was tuned to 720 nm for glutamate uncaging. The imaging power for two lasers was controlled independently by electro-optical modulators (Conoptics). The fluorescence was collected by an objective (60X, 1.0 numerical aperture, Olympus), separated by a dichroic mirror (Chroma, 565 nm for mEGFP/mCherry and 505 nm for mTurquoise2/mVenus), filtered by wavelength filters (Chroma, ET520/60M-2p for mEGFP, ET620/60M-2p for mCherry, ET480/40M-2p for mTurquoise2, ET535/50M-2p for mVenus), and finally detected by two independent photoelectron multiplier tubes (PMTs). We used 1.2-1.5 mW imaging power for mEGFP/mCherry sensor, and 1.6-1.8 mW for mTurquoise2/mVenus sensor.

Two-photon fluorescence lifetime imaging in HEK 293T cells was performed in imaging solution containing 20 mM HEPES (pH 7.3), 130 mM NaCl, 2.5 mM KCl, 2 mM $MgCl_2$, 2 mM $NaHCO_3$, 1.25 mM NaH_2PO_4 and 25 mM D-glucose.

Two-photon lifetime imaging and glutamate uncaging in organotypic slices was performed in Mg^{2+}-free artificial cerebrospinal fluid (ACSF; 127 mM NaCl, 2.5 mM KCl, 1.25 mM NaH_2PO_4, 25 mM $NaHCO_3$, 25 mM D-glucose, aerated with 95% O_2 and 5% CO_2) with 4 mM $CaCl_2$, 4 mM MNI-caged glutamate (Tocris) and 1 μM tetrodotoxin (TTX, Enzo). Uncaging pulses (0.5 Hz, 60 s, 4-6 ms, 3.5-3.8 mW) were delivered to the back focal aperture of the objective, which was around 0.5 μm from the tip of the spine head. The adjacent spine refers to the first or second spine located next to the stimulated spine, typically positioned opposite the stimulated spine. Additionally, the size of the adjacent spine must be sufficiently large for imaging. We used a heater controller (Warner Instruments TC-344B) to monitor the temperature at 25-27°C or 33-35°C. For pharmacological experiments, inhibitors or vehicles were applied in ACSF 30 min before experiments. Please note that **Fig. 2b,e** include control samples from **Fig. 2c-g**, and **Fig. 3b,e** include control samples from **Fig. 3c-g**. Images were analyzed by MATLAB (MathWorks) and ImageJ.

2pFLIM data analysis

As described previously[58], the fraction of donor bound to acceptor was determined by fitting a fluorescence lifetime curve that summed contributions from all pixels in the image, using a double exponential function convolved with the Gaussian pulse response function, as shown in the

equation:

$$F(t) = F_0[P_D H(t, t_0, \tau_D, \tau_G) + P_{AD} H(t, t_0, \tau_{AD}, \tau_G)]$$

In this equation, F_0 is the peak fluorescence before convolution, while P_D and P_{AD} represent the fractions of free donor and donor bound to the acceptor, respectively. t_0 is the time offset, τ_D is the fluorescence lifetime of the free donor, τ_{AD} is the fluorescence lifetime of donor bound with acceptor, τ_G defines the width of the Gaussian pulse response function, and $H(t)$ is a fluorescence lifetime curve with a single exponential function convolved with the Gaussian pulse response function:

$$H(t, t_0, t_D, t_G) = \frac{1}{2}\exp\left(\frac{\tau_G^2}{2\tau_D^2} - \frac{t-t_0}{\tau_D}\right) erfc\left(\frac{\tau_G^2 - \tau_D(t-t_0)}{\sqrt{2}\tau_D\tau_G}\right)$$

in which erfc is the complementary error function. We fixed τ_D as 2.46 ns, 2.60 ns and 4.15 ns, corresponding to the free mEGFP–Rab4a, mEGFP-Rab10, and mTurquoise2-Rab10 donors, respectively. Similarly, τ_{AD} was set to the fluorescence lifetime of the donor when bound to its acceptor, with values of 1.10 ns for the mEGFP/mCherry pair and 1.60 ns for the mTurquoise2/mVenus pair.

To create the fluorescence lifetime image, we computed the mean photon arrival time, $< t >$, for each pixel using the following equation:

$$< t > = \int tF(t)dt / \int F(t)dt$$

The mean photon arrival time is then related to the mean fluorescence lifetime, $< \tau >$, by an offset arrival time, t_0, which is determined through image-wide fitting:

$$< \tau > = < t > - t_0$$

For small regions of interest (ROIs) within an image, such as spines or dendrites, the binding fraction (P_{AD}) was calculated using the formula:

$$P_{AD} = \frac{\tau_D(\tau_D - < \tau >)}{(\tau_D - \tau_{AD})(\tau_D + \tau_{AD} - < \tau >)}$$

Spine volume measurement

To estimate the spine volume in neurons expressing Rab sensors, we measured the integrated fluorescence intensity of mCherry-RBD-mCherry or mVenus-RBD-mCherry in the spine, which is proportional to the spine volume[88], and normalized it by the fluorescence intensity in the thick apical dendrite from the same neuron. We further multiplied this normalized value by the volume of the point spread function, which gives the spine volume in fL[58,89].

For the sensor experiments, we used mCherry as a volume indicator. We acknowledge that contributions from bleed-through from mEGFP-Rab (approximately 3%) and FRET changes (around 20%) could affect the volume measurements. However, since we observed similar fluorescence changes in both the green and red channels, we believe these factors have a minimal impact on our results (**Extended Data Fig. 6a, d**).

NMDA application

Rat organotypic hippocampal slices (DIV 9-DIV 13) were biolistically transfected with indicated Rab sensors. After 3-4 day expression, CA1 pyramidal neurons were imaged in the basal solution (ACSF with 2 mM $CaCl_2$, 2 mM $MgCl_2$ and 1 µM TTX) for 6 min. NMDA (Tocris) was bath-applied in

the zero Mg^{2+} solution (ACSF with 4 mM $CaCl_2$, 15 μM NMDA and 1 μM TTX) for 2 min, and replaced by the washout solution (ACSF with 2 mM $CaCl_2$, 2 mM $MgCl_2$, 1 μM TTX and 50 μM AP5) for 32 min.

sLTP measurement

Rat organotypic hippocampal slices were biolistically transfected with indicated constructs at days *in vitro* 9-13 (DIV 9-DIV 13). The constructs for Rab shRNA knockdown experiments were: scrambled shRNA/mEGFP (Ctrl shRNA); Rab4a shRNA/mEGFP and Rab4b shRNA/mEGFP (Rab4a/4b shRNA); Rab4a shRNA/mEGFP, Rab4b shRNA/mEGFP, and pCAGGS-mCherry-shRNA-resistant Rab4a (Rab4a rescue); Rab10 shRNA/mEGFP (Rab10 shRNA); Rab10 shRNA/mEGFP and pCAGGS-mCherry-shRNA-resistant Rab10 (Rab10 rescue). The constructs for DN- and CA-Rab overexpression experiments were: pCAGGS-mEGFP (Ctrl); pCAGGS-mEGFP and pCAGGS-mCherry-Rab DN (Rab DN); pCAGGS-mEGFP and pCAGGS-mCherry-Rab CA (Rab CA).The constructs were expressed for 4-5 days for Rab shRNA knock-down, and 2-3 days for DN- or CA-Rab mutant overexpression. CA1 pyramidal neurons were imaged in ACSF (aerated with 95% O_2 and 5% CO_2) with 4 mM $CaCl_2$, 4 mM MNI-caged glutamate and 1 μM TTX. Two-photon glutamate uncaging (0.5 Hz, 60 s, 4-6 ms, 3.5-3.8 mW) was performed at a single spine. All experiments were paired with the same day controls from the same batch of slices. The acquired images were analyzed by MATLAB (MathWorks).

Organotypic hippocampal slices of $Rab10^{fl/fl}$ mice slices were biolistically transfected with tdTomato-Cre and mEGFP, or tdTomato and mEGFP as a control at DIV 10. At DIV 14, CA1 pyramidal neurons were imaged in ACSF (aerated with 95% O_2 and 5% CO_2) with 4 mM $CaCl_2$, 4 mM MNI-caged glutamate and 1 μM TTX. Two-photon glutamate uncaging (0.5 Hz, 60 s) was performed at a single spine. All experiments were paired with the same day controls from the same batch of slices. The acquired images were analyzed by MATLAB (MathWorks).

Spine size and spine density measurement

Rat organotypic hippocampal slices were biolistically transfected with indicated constructs at DIV 9. The constructs for Rab shRNA knockdown experiments were: scrambled shRNA/mEGFP (Ctrl shRNA), Rab4a shRNA/mEGFP and Rab4b shRNA/mEGFP (Rab4a/4b shRNA), or Rab10 shRNA/mEGFP (Rab10 shRNA). After 4 days expression, CA1 pyramidal neurons were imaged in ACSF by two photon microscopy at 25-27°C. All experiments were paired with the same day controls from the same batch of slices. The acquired images were analyzed by MATLAB (MathWorks) and ImageJ.

Activity-dependent SEP-GluA1 exocytosis

Rat organotypic hippocampal slices were biolistically transfected with indicated constructs at DIV 9-DIV 13. The DNA constructs for each condition were: pCAGGS-mCherry, SEP-GluA1, and scrambled shRNA (Ctrl shRNA); pCAGGS-mCherry, SEP-GluA1, and pCAGGS-3Flag-TeTxLC (TeTxLC); pCAGGS-mCherry, SEP-GluA1, Rab4a shRNA, and Rab4b shRNA (Rab4a/4b shRNA); pCAGGS-mCherry, SEP-GluA1, and Rab10 shRNA (Rab10 shRNA); pCAGGS-mCherry, SEP-GluA1, Rab4a shRNA, Rab4b shRNA, and pCAGGS-3Flag-shRNA-resistant Rab4a (Rab4a rescue); pCAGGS-mCherry, SEP-GluA1, Rab10 shRNA, and pCAGGS-3Flag-shRNA-resistant Rab10 (Rab10 rescue). After 4 days expression, CA1 pyramidal neurons were imaged in ACSF (aerated with 95% O_2 and 5% CO_2) with 4 mM $CaCl_2$, 4 mM MNI-caged glutamate and 1 μM TTX at 25-27°C. All experiments were paired with the same day controls from the same batch of slices. After taking five baseline images of a secondary apical dendrite (1 min interval) with 1.2-1.5 mW imaging laser power, we bleached the whole dendrite by increasing the imaging laser power to 4.0-4.5 mW for 2 min. We then performed two-photon glutamate uncaging (0.5 Hz, 60 s, 4-6 ms, 3.5-3.8 mW) at a single spine and collected eight images (1 min interval). The acquired images were analyzed by MATLAB (MathWorks) and ImageJ.

In **Extended Data Fig. 14**, we addressed the impact of SEP-GluA1's lateral diffusion by subtracting the change in spine surface area (Volume$^{2/3}$) rather than correcting for spine volume. This approach is necessary because SEP-GluA1 is only fluorescent on the cell surface, while the fluorescence intensity of cytosolic proteins such as mCherry is proportional to spine volume. Therefore, the overall fluorescence change (ΔF) should be addition of the contribution from AMPAR trafficking (ΔF_t) and the change in surface area (ΔS) multiplied by the remaining SEP-GluA1 fluorescence per unit area (f):

$$\Delta F = \Delta F_t + f\Delta S$$

Since fluorescence immediately after photobleaching (before AMPAR trafficking happens), F_o, is given by fS (S is the surface area of the spine):

$$\Delta F/F_o = \Delta F_t/F_o + f\Delta S/fS$$

$$= \Delta F_t/fS + \Delta S/S$$

Assuming that the surface area change ($\Delta S/S$) is the volume change ($\Delta V/V$) to the power of 2/3, the contribution of the AMPAR trafficking can be calculated as:

$$\Delta F_t/F = \Delta F/F - (\Delta V/V)^{2/3}$$

Thus, we obtained the contribution of AMPAR trafficking by subtracting the volume change ($\Delta V/V$) to the power of 2/3 from the fluorescence recovery ($\Delta F/F$).

Validation of SLENDR-mediated Rab10 knockin

The SLENDR technique was as previously described[59]. Briefly, Rab10 sgRNA (IDT) was ligated into the sgRNA scaffold of pX330[90] to generate Rab10 sgRNA-expressing plasmid. Rab10 sgRNA-expressing plasmid and single-stranded oligodeoxynucleotides (ssODNs; IDT) for homology-directed repair (HDR) were transfected into Neuro 2a cells by electroporation. Genomic DNA from the electroporation-transduced Neuro 2a cells was isolated with DNeasy Blood & Tissue Kit (Qiagen) following the manufacturer's instruction. Genomic PCR was performed using extracted DNA as a template with corresponding primer set. The PCR product was purified by QiaQuick gel extraction kit (Qiagen) and then proceeded to Sanger sequencing to detect 2XHA insertion.

sgRNA target sequences (5'-3')

Rab10: ACGTCTTCTTCGCCATTGGGAGG Rab4a: GCGGAGCTGTGGCGGCAGAA

ssODNs sequence (5'-3', upper case: 2XHA tag sequence)

ggagttggttgtagtgagcagttccgatcccttggggctaccggcggcgagcgcccgagccgctcctcccaatgTACCCATACGATGTTCCAGATTAC

Rab10 primer set, recombination

Rab10-2xHA-Fw: GCTCCTCCCAATGTACCCAT

Rab10-RV: AGAAACCGGATTCTGGAACG

Rab10 primer set, control

Rab10-FW: TTTCAAGCTGCTCCTGATCG

Rab10-RV: AGAAACCGGATTCTGGAACG

In Utero Electroporation and histology for SLENSR-mediated Rab10 knockin

In utero electroporation (IUE) was performed as previously described[59]. Electroporation was performed at E13-E14 in anesthetized mice. For endogenous Rab10 localization, 1-2 µl mixture of plasmids (pX330-Rab10 sgRNA and pPB-CAG-mEGFP, 1µg/µl) and ssODNs (20 µM) was injected into the lateral ventricle of each pup. For colocalization examination of endogenous Rab10 and endosomal makers, 1-2 µl mixture of plasmids (pX330-Rab10 sgRNA and pCAGGS-mEGFP-Rab5a, pCAGGS-mEGFP-Rab7a or pCAGGS-mCherry-Rab11a, 1µg/µl) and ssODNs (20 µM) was injected into the lateral ventricle of each pup.

With ketamine-xylazine anesthesia (100 µg of ketamine -10 µg of xylazine per g of body weight, i.p.), mice were perfused with 4% paraformaldehyde in 0.1 M phosphate buffer, pH 7.4, and the brain was fixed for 4–12 h. After wash with PBS, coronal vibratome sections (50 µm in thickness) were prepared (VT1200, Leica). For immunohistochemistry, slices were permeabilized with 0.3-0.4% Triton X-100 in PBS, blocked with 5% normal goat serum and 2% BSA or 5% normal donkey serum in PBS, and incubated overnight with rabbit anti-HA primary antibody (1:1000, Cell Signaling Technology). After 1–3 h incubation with Alexa Fluor-conjugated secondary antibodies (Invitrogen) followed by DAPI staining (0.1 µg/ml, Life technologies), slices were imaged using a confocal laser-scanning microscope (LSM880 with Airyscan, Zeiss). Images were processed and analyzed using the Zen (Zeiss) and the Fiji softwares.

Dual-luciferase reporter assay

HEK 293T cells were plated into 24-well plates and cotransfected with psiCHECK-2-Rab GTPases and the respective shRNA at a 1:3 ratio. For positive control, we used shRNA against hRluc with the following sequence: TCATAGTAGTTGATGAAGGAG (mature antisense). After 48 hours transfection, luciferase activity was measured using the Dual-Luciferase Reporter Assay System (Promega) following the manufacturer's protocol. After removing the culture medium, cells were briefly rinsed in pre-warmed 0.1M phosphate-buffered saline (PBS), and lysed in 100µL of 1X passive lysis buffer in the luciferase assay kit. After gently shaking for 15 min at room temperature, samples were prepared in a 96-well plate for luminescence measurement using the GloMax-Multi Detection System (Promega). For data analysis, the hRluc (firefly luciferase) luminescence was normalized by the hluc+ (*Renilla* Luciferase) luminescence in each well to control for transfection efficiency. All experiments were paired with the same day controls from the same batch of HEK 293T cells.

Lentivirus infection in dissociated neuron cultures

Dissociated postnatal cortical cultures were prepared as previously published[82]. Proliferation of non-neuronal cells was inhibited by adding Cytosine arabinoside (2.5 µM) at DIV 2. At DIV 6 cultures were infected with lentiviral particles containing Rab4a shRNA/mEGFP (Rab4a shRNA); Rab4b shRNA/mEGFP (Rab4b shRNA); Rab4a shRNA/mEGFP and Rab4b shRNA/mEGFP (Rab4a/4b shRNA); Rab10 shRNA/mEGFP (Rab10 shRNA) or scrambled shRNA/mEGFP (Ctrl shRNA). At DIV 17 cells were washed with ice-cold PBS and immediately extracted with ice-cold T-PER protein extraction buffer (Pierce) supplemented with inhibitors for proteases and phosphatases (Roche). The lysates were centrifuged at 15000 g for 15 minutes at 4°C and the supernatants were used for further analysis.

SDS-PAGE and immunoblotting

Samples were prepared for standard SDS-PAGE and separated on 12% acrylamide gel (Mini-PROTEAN TGX precast gels, Bio-Rad), then transferred onto 0.2 µm pore size PVDF membranes (Millipore) using semi-dry immunoblotting (transfer buffer containing 25 mM Tris, 200 mM glycine and 20% methanol). Membranes were blocked with 5% nonfat milk (Great Value) in TBS-T

(Tris Buffered Saline with 0.1% Tween-20) for 1 hour at room temperature, then incubated overnight at 4°C with primary antibodies diluted in 5% BSA in TBS-T. We used the following commercially available antibodies: rabbit anti-Rab10 (1:500; Cell Signaling Technology), rabbit anti-Rab4b (1:500; ThermoFisher Scientific), mouse anti-Rab4a (1:500; ThermoFisher Scientific) and mouse anti-β-actin (1:2000; Sigma). Membranes were washed 3 times for 15 minutes in TBS-T, followed by incubation for 2 hours at room temperature with HRP-conjugated goat anti-rabbit or goat anti-mouse secondary antibodies (Bio-Rad), diluted 1:5000 in 5% nonfat milk in TBS-T. Membranes were washed 3 times for 15 minutes in TBS-T, then incubated with Pierce ECL Plus western blotting substrate (for Rab10, Rab4a and Rab4b) or Pierce ECL western blotting substrate (for β-actin) for detection of western blotted proteins. We used the Image Quant LAS4000 Imaging System (GE Healthcare) to visualize protein bands.

Acute slice preparation

Rab 10 Cre – and Cre + littermate mice (P 30-P 50) were anesthetized by isoflurane inhalation and perfused intracardially with a chilled choline chloride solution. The brain was removed and placed in the same choline chloride solution composed of 124 mM Choline Chloride, 2.5 mM KCl, 26 mM $NaHCO_3$, 3.3 mM $MgCl_2$, 1.2 mM NaH_2PO_4, 10 mM Glucose, and 0.5 mM $CaCl_2$, pH 7.4 equilibrated with 95% O_2 and 5% CO_2. Coronal slices (300 µm) containing the hippocampus were cut using a vibratome (Leica) and maintained in a submerged chamber at 32 °C for 1 h and then at room temperature in oxygenated ACSF.

Electrophysiology

Slices were perfused with oxygenated ACSF containing 2 mM $CaCl_2$, 2 mM $MgCl_2$ and 100 µM picrotoxin. One glass electrode (resistance ~4 MΩ) containing the same ACSF solution was placed in the dendritic layer of CA1 area (~100–200 µm away from the soma) while stimulating Schaffer Collateral fibers with current square pulses (0.1 ms) using a concentric bipolar stimulation electrode (FHC). The initial slope of the fEPSP was monitored with custom software (Matlab). The stimulation strength was set to ~50% saturation. A 20 min stable baseline was first recorded before induction of LTP. LTP was induced by applying 5 trains of TBS. One TBS train consists 10 bursts of 4 stimulations at 100 Hz. The inter-burst interval is 200 ms and the interval between trains is 2 s. fEPSPs responses were recorded for an hour after the stimulation protocol. All data were analyzed with an in-house program written with Matlab. Data are presented as mean ± SEM.

Whole cell recording

Animals were sedated by isoflurane inhalation, and perfused intracardially with ice-cold choline chloride solution containing 124 mM choline chloride, 2.5 mM KCl, 26 mM $NaHCO_3$, 3.3 mM $MgCl_2$, 1.2 mM NaH_2PO_4, 10 mM Glucose and 0.5 mM $CaCl_2$ (pH 7.4 equilibrated with 95% O_2 and 5% CO_2). Brains were then removed and placed in the same chilled choline chloride solution and coronal acute slices of 300 µm from left and right hemispheres were collected and placed in oxygenated (95% O_2 and 5% CO_2) ACSF (in mM: NaCl 127, KCl 2.5, Glucose 10, $NaHCO_3$ 25, NaH_2PO_4 1.25, $MgCl_2$ 2, $CaCl_2$ 2 mM) at 32°C for 1 h and maintained at room temperature for the rest of the experiment. Whole cell voltage clamp recordings of hippocampal neurons of Cre+ and Cre-Rab10 animals were made with a Multiclamp 700B. Patch pipettes (3-6 ΩM) were filled with a Cs Methanesulfonate solution (in mM: Cs $MeSO_4$ 120, NaCl 5, TEA-Cl 10, HEPES 5, QX314-Br 5, EGTA 5, NaATP 4, MgGTP 0.3, pH 7.4). Experiments were performed at room temperature (18-20°C) and slices were perfused with oxygenated ACSF (in mM: NaCl 127, KCl 2.5, Glucose 10, $NaHCO_3$ 25, NaH_2PO_4 1.25, $MgCl_2$ 2, $CaCl_2$ 2 mM, picrotoxin 100 µM). AMPAR and NMDAR evoked responses were measured clamping the cells at -70 mV and +40 mV, respectively. Postsynaptic currents were evoked by electrical stimulation using a concentric bipolar electrode (THC), with a pulse of 0.1 ms. Input-output curves were first assessed by changing the stimulation intensity from 0 to 200 µA. For the rest of the recordings, the stimulation intensity was set to the amplitude that elicited a 50% of EPSC response.

Recordings were filtered at 2 kHz and digitized at 10 kHz. Series and input resistances were monitored throughout the experiment. All data were acquired and analyzed with an in-house program written in Matlab. Data are presented as mean ± SEM.

Quantification and statistical analysis

Results are reported as mean ± SEM. Statistical analysis was performed with GraphPad Prism 7 and 10. Comparisons between two groups were performed using unpaired two-tailed Student's t-tests (* $p<0.05$, ** $p<0.01$, *** $p<0.001$, **** $p<0.0001$). Comparisons for more than two groups were calculated using one-way ANOVA followed by Bonferroni's multiple comparison tests or two-way ANOVA (* $p<0.05$, ** $p<0.01$, *** $p<0.001$, **** $p<0.0001$).

Acknowledgements

This work was supported by grants from JSPS Overseas Research Fellowship (667 (JN)), NRF (NRFF12-2020-0008 (JN)), NIH (NS068410 (RY), MH080047 (RY), MH095090 (JN and RY)), HHMI (RY) and Max Planck Florida Institute for Neuroscience. We thank Drs. Sridhar Raghavachari, Scott Soderling, Fan Wang, and Anne West for important discussions. We thank Dr. Scott Soderling for SEP-GluA1 plasmid. We thank Dr. Boris Kantor and Marguerita Klein at Duke University Viral Vector Core for lentivirus production, Dr. Long Yan and light microscopy facility at Max Planck Florida Institute for technical support, David Kloetzer for laboratory management and Dr. Lesley Colgan for critical reading of the manuscript. We thank all other Yasuda Lab members for discussions.

Additional information

Author contributions

JW, JN and RY designed experiments. JW performed most experiments. JN contributed to the general design and optimization scheme for Rab sensors. JW developed sensors for Rab4, 7 and 10. JN developed sensors for Rab5 and 8. PP performed electrophysiological recordings. EO performed structural plasticity measurements in Rab10 cKO mice. XL examined the localization of endogenous Rab10 by the SLENDR technique. TEM contributed Rab10 cKO mice. EMS performed western blot experiments. GO, TW and IS contributed technically. JW and RY wrote the manuscript with inputs from all authors.

Extended Data

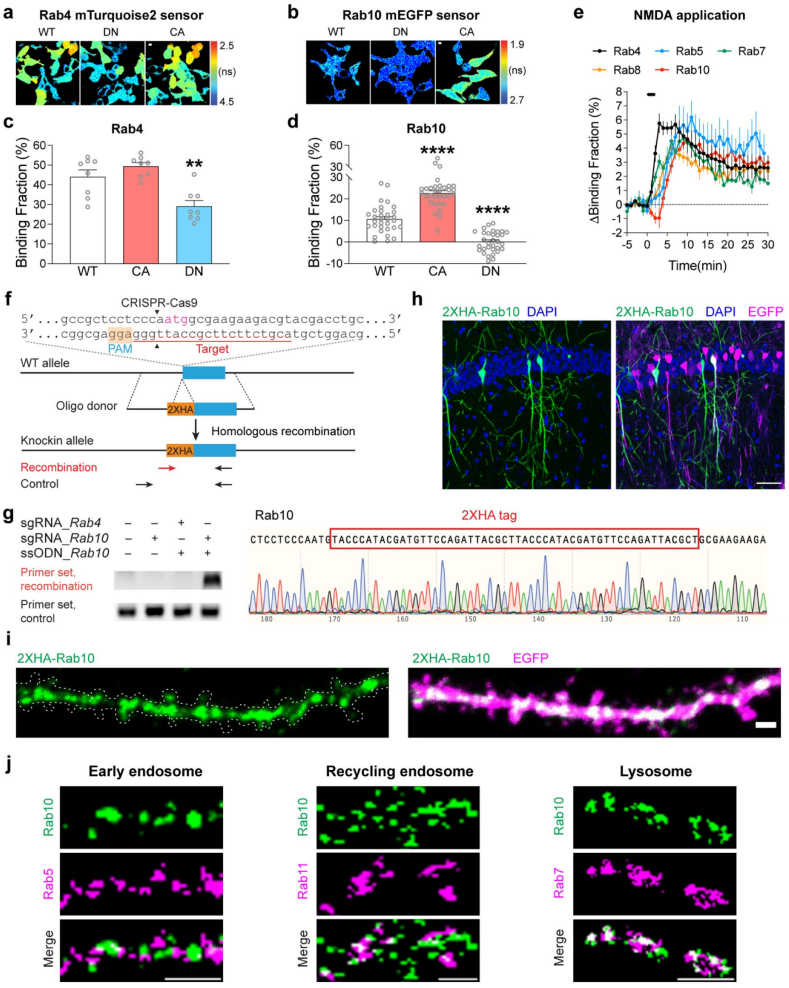

Extended Data Fig. 1

mTurquoise2-Rab4 and mEGFP-Rab10 FRET sensors in HEK 293T Cells, all Rab sensor activity changes upon NMDA application, and localization of endogenous Rab10.

(a) Representative fluorescence lifetime images of HEK 293T cells transfected with mTurquoise2-Rab4 sensors. Scale bars represent 5 μm. **(b)** Representative fluorescence lifetime images of HEK 293T cells transfected with mEGFP-Rab10 sensors. Scale bars represent 5 μm. **(c)** Binding fraction of mTurquoise2-Rab4 sensors. Data represent mean ± SEM (** p<0.01, one-way ANOVA followed by Bonferroni's multiple comparison tests). N=8, 8, and 8 from left to right. **(d)** Binding fraction of mEGFP-Rab10 sensors. Data represent mean ± SEM (**** p<0.0001, one-way ANOVA followed by Bonferroni's multiple comparison tests). N=32, 32, and 32 from left to right. **(e)** Averaged time courses of Rab sensor binding fraction change by NMDA application in rat hippocampal CA1 pyramidal neurons. Data represent mean ± SEM. N=4-11 for each group. **(f)** Schematics of HA-tag knockin into endogenous Rab10 by SLENDR technique. Mouse genomic loci of Rab10 shows the target sites for Cas9, sgRNA and ssODNs. The sgRNA target regions and PAM sequences are labelled with red and orange, respectively. The start codons are marked with magenta. The Cas9 cleavage sites are indicated by black arrowheads. The recombination and control primer sets are in arrows. **(g)** Validation of SLENDR-mediated 2XHA tag insertion into endogenous Rab10. Left: PCR genotyping in genomic DNA extracted from Neuro 2a cells electroporated with indicated sgRNA and ssODNs. Right: Sanger sequencing demonstrated the knockin of 2XHA tag to the N-terminus of endogenous Rab10. **(h)** Confocal microscopic images of the hippocampal CA1 region at P37 stained with DAPI (blue), HA tag fused to the N-terminus of endogenous Rab10 (green) and EGFP (magenta). Scale bar is 50 μm. **(i)** Representative images of the secondary apical dendrites of CA1 pyramidal neurons stained with HA tag fused to the N-terminus of endogenous Rab10 (green) and EGFP (magenta). Scales bar is 1 μm. **(j)** Representative images of endogenous Rab10 (green, SLENDR-mediated 2XHA tag knockin) and exogenous endosomal markers (magenta) in dendrites of CA1 pyramidal neurons. Exogenously expressed mEGFP-Rab5a, mCherry-Rab11a and mEGFP-Rab7 were used as markers for early endosome, recycling endosome and lysosome, respectively. Scales bars are 1 μm.

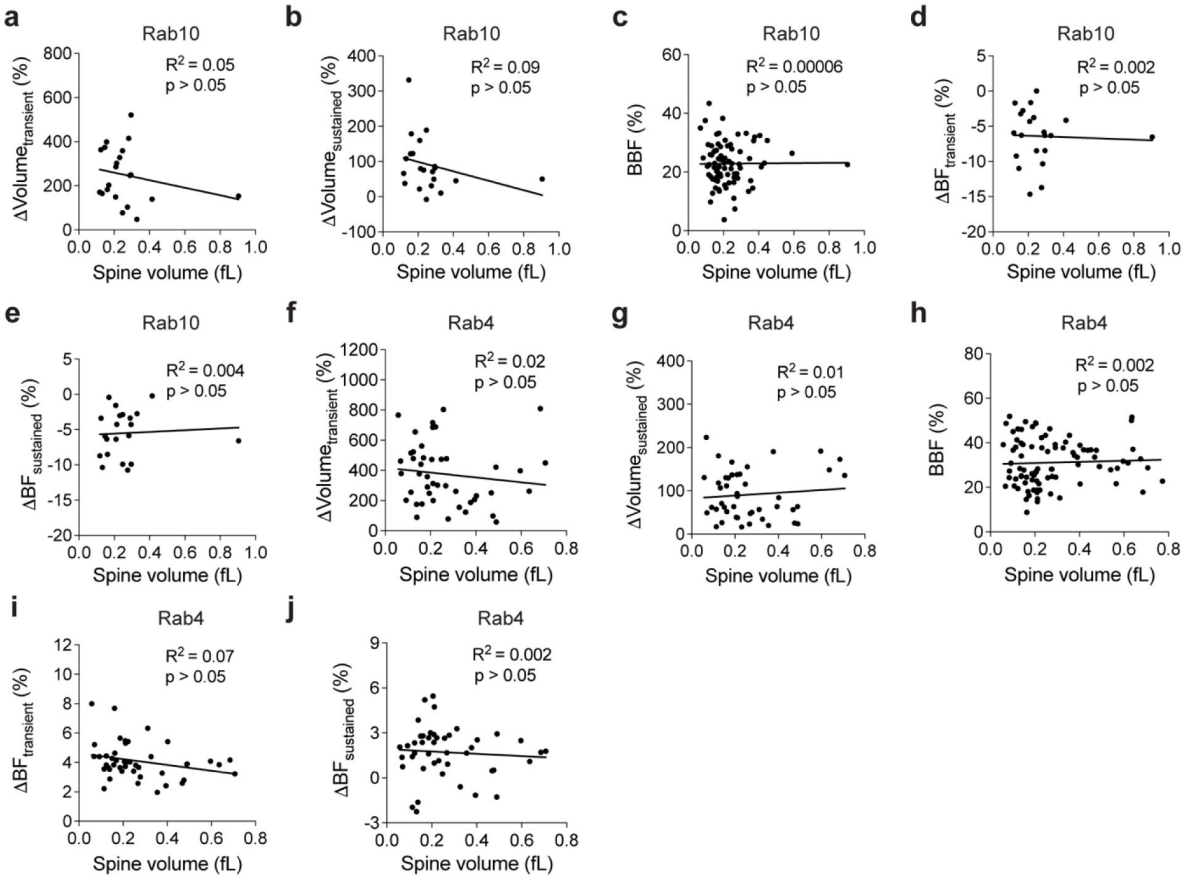

Extended Data Fig. 2

Relationship between initial spine volume and basal Rab GTPase activity, spine volume change or activity change during sLTP.

(a and b) Relationship between the initial spine volume and spine volume changes during the transient (a, averaged over 1.3-4 min) or sustained phase (b, averaged over 19-31 min) in neurons expressing Rab10 sensor. N=21/20 (spine/neuron). No significant correlation ($p > 0.05$) was found. **(c)** Relationship between spine volume and basal binding fraction (BBF) of Rab10 sensor. N=81/20 (spine/neuron). No significant correlation ($p > 0.05$) was found. **(d and e)** Relationship between the initial spine volume and changes in binding fraction of Rab10 sensor during the transient (d, averaged over 1.3-4 min) or sustained phase (e, averaged over 19-31 min) of sLTP in the stimulated spines. N=21/20 (spine/neuron). No significant correlation ($p > 0.05$) was found. **(f and g)** Relationship between the initial spine volume and spine volume changes during the transient (f, averaged over 1.3-4 min) or sustained phase (g, averaged over 19-31 min) in neurons expressing Rab4 sensor. N=42/34 (spine/neuron). No significant correlation ($p > 0.05$) was found. **(h)** Relationship between spine volume and basal binding fraction (BBF) of Rab4 sensor. N=90/39 (spine/neuron). No significant correlation ($p > 0.05$) was found. **(i and j)** Relationship between the initial spine volume and Rab4 activity changes during the transient (i, averaged over 1.3-4 min) or sustained phase (j, averaged over 19-31 min) of sLTP in the stimulated spines. N=42/34 (spine/neuron). No significant correlation ($p > 0.05$) was found.

Extended Data Fig. 3

Binding fraction changes of mTurquoise2-Rab10 paired with false acceptor during sLTP.

(a) Averaged time course of changes in binding fraction of Rab10 sensor (Ctrl, black) in the stimulated spines during sLTP. When mTurquoise2-Rab10 was paired with a false acceptor (False, red), mVenus-Rabenosyn5 [439-503]-mVenus, little activity change was observed. Data represent mean ± SEM. N=7/7 and 14/9 (spine/neuron) for Ctrl and False, respectively. **(b)** Quantification of changes in binding fraction during the transient phase (1.3-4 min) and sustained phase (19-31 min) for the same experiments as in (a). Data represent mean ± SEM (**** p<0.0001, Student's t-tests). **(c)** Averaged time courses of changes in spine volume for the same experiments as in (a). Data represent mean ± SEM. **(d)** Quantification of changes in spine volume during the transient phase (1.3-4 min) and sustained phase (19-31 min) for the same experiments as in (a). Data represent mean ± SEM (n.s., not significant, Student's t-tests). Please note the quantification data in (b) and (d) are also presented in **Fig. 2c,d,f,g**.

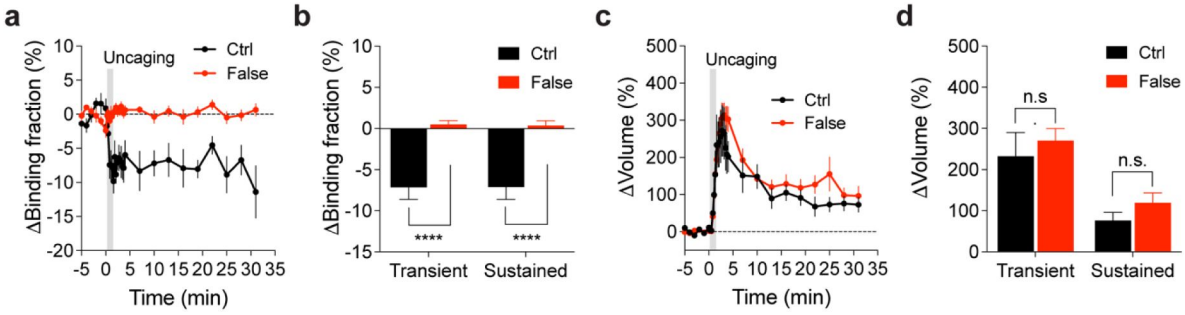

Extended Data Fig. 4

Inactivation of Rab10 during sLTP induced at near physiological temperature.

(a) Averaged time courses of changes in binding fraction of Rab10 sensor in the stimulated spines during sLTP at 25-27°C (black) and 33-35°C (red). Data represent mean ± SEM. N=49/42 and 14/12 (spine/neuron) for 25-27°C and 33-35°C, respectively. **(b)** Quantification of changes in binding fraction in the transient phase (1.3-4 min) and sustained phase (19-31 min) for the same experiments as in (a). Data represent mean ± SEM (n.s., not significant, Student's t-tests). **(c)** Averaged time courses of changes in spine volume for the same experiments as in (a). Data represent mean ± SEM. **(d)** Quantification of changes in spine volume during the transient phase (1.3-4 min) and sustained phase (19-31 min) for the same experiments as in (a). Data represent mean ± SEM (n.s., not significant, Student's t-tests). Please note that the 25-27°C (black) samples in (a-d) are the same as those in **Fig. 2b, e**.

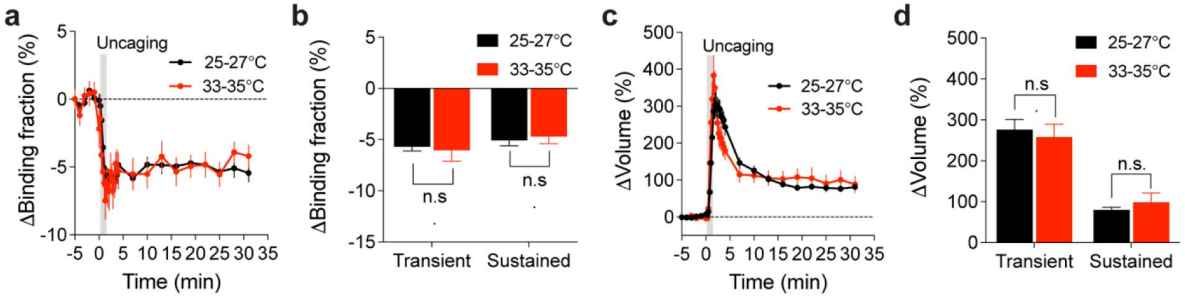

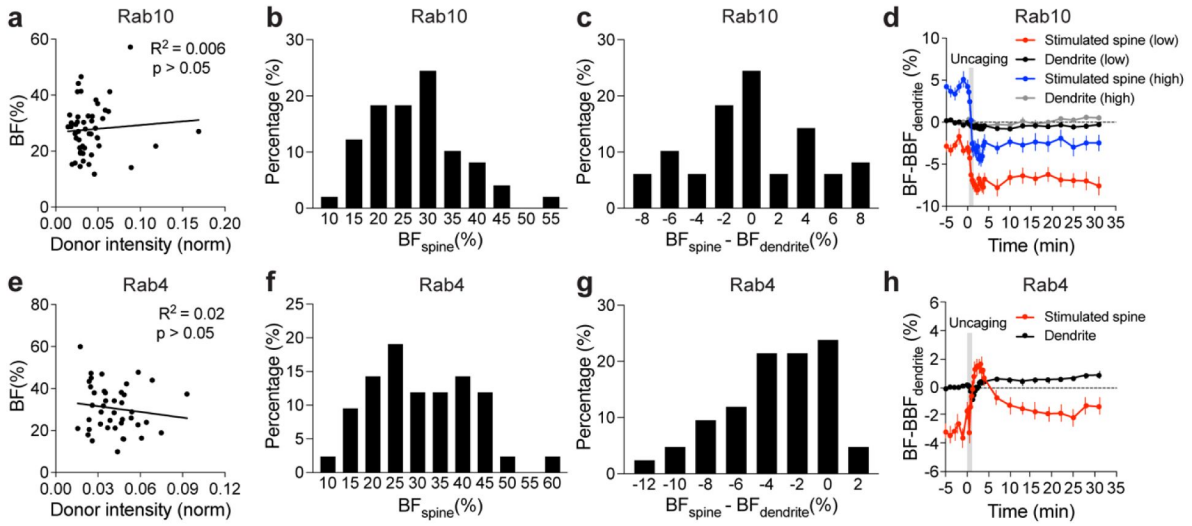

Extended Data Fig. 5

Properties of basal binding fraction and binding fraction change in the stimulated spines for Rab10 and Rab4 sensors.

(a) Relationship between normalized donor intensity and spine binding fraction (BF) for Rab10 sensor. N=49/42 (spine/neuron). No significant correlation ($p > 0.05$) was found. **(b)** Frequency distribution of basal binding fraction in the stimulated spines (BF_{spine}) for Rab10 sensor. N=49/42 (spine/neuron). **(c)** Frequency distribution of basal binding fraction difference between the spines and dendrite (BF_{spine} - $BF_{dendrite}$) for Rab10 sensor. N=49/42 (spine/neuron). **(d)** Averaged time course of binding fraction (BF) subtracted by basal binding fraction (BBF) of dendrite for the stimulated spines and dendrite in Rab10 sensor expressing neurons. For spines with a higher BF (high, blue) than the dendrite (high, gray), Rab10 activity decreased to a level lower than that of the dendrite during sLTP. Data represent mean ± SEM. N=21/18 (spine/neuron). For spines with a lower BF (low, red) than the dendrite (low, black), Rab10 activity still decreased during sLTP. Data represent mean ± SEM. N=28/24 (spine/neuron). **(e)** Relationship between normalized donor intensity and spine binding fraction for Rab4 sensor. N=42/34 (spine/neuron). No significant correlation ($p > 0.05$) was found. **(f)** Frequency distribution of basal binding fraction in the stimulated spines for Rab4 sensor. N=42/34 (spine/neuron). **(g)** Frequency distribution of basal binding fraction difference between the spines and dendrite for Rab4 sensor. N=42/34 (spine/neuron). **(h)** Averaged time course of binding fraction subtracted by basal binding fraction of dendrite for the stimulated spines and dendrite in Rab4 sensor expressing neurons. Data represent mean ± SEM. N=42/34 (spine/neuron).

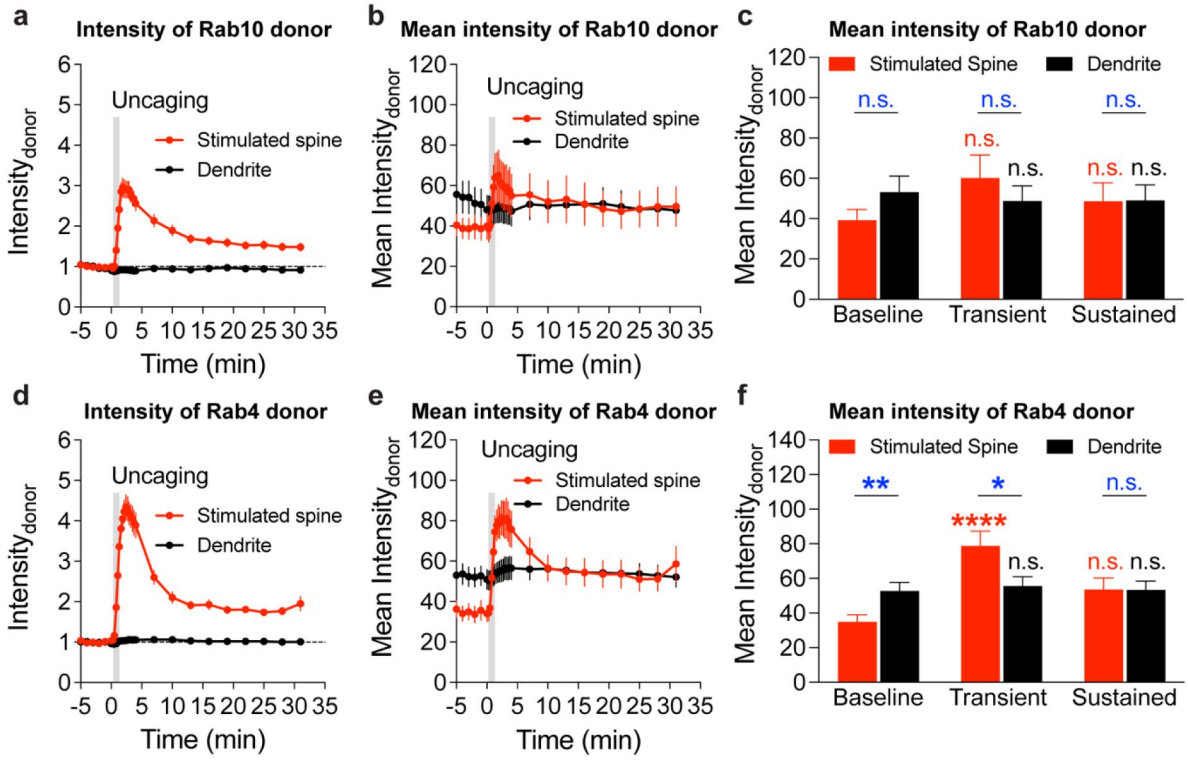

Extended Data Fig. 6

Intensity and mean intensity of Rab10 and Rab4 sensor donors in the stimulated spines and dendrites during sLTP.

(a and b) Averaged time courses of Rab10 donor intensity (a) and mean intensity (b) in the stimulated spines (red) and dendrites (black) during sLTP. Data represent means ± SEM. N=49/42 (spine/neuron) and 49/42 (dendrite/neuron) for the stimulated spine and dendrite, respectively. **(c)** Quantification of Rab10 donor mean intensity in the baseline (averaged over -5-0 min), transient phase (averaged over 1.3-4 min) and sustained phase (averaged over 19-31 min) for the experiments in (b). Data represent means ± SEM. Red color statistics indicate comparisons with baseline in the stimulated spines, and black color statistics indicate comparisons with baseline in the dendrites (n.s., not significant, two-way ANOVA). Blue color statistics indicate comparisons between the stimulated spines and dendrites (n.s., not significant, Student's t-tests). **(d and e)** Averaged time courses of Rab4 donor intensity (d) and mean intensity (e) in the stimulated spine (red) and dendrite (black) during sLTP. N=42/34 (spine/neuron) and 42/34 (dendrite/neuron) for the stimulated spine and dendrite, respectively. **(f)** Quantification of Rab4 donor mean intensity in the baseline (averaged over -5-0 min), transient phase (averaged over 1.3-4 min) and sustained phase (averaged over 19-31 min) for the experiments in (e). Data represent means ± SEM. Red color statistics indicate comparisons with baseline in the stimulated spines and black color statistics indicate comparisons with baseline in the dendrites (n.s., not significant, **** $p<0.0001$, two-way ANOVA). Blue color statistics indicate comparisons between the stimulated spines and dendrites (n.s., not significant, * $p<0.05$, ** $p<0.01$, Student's t-tests).

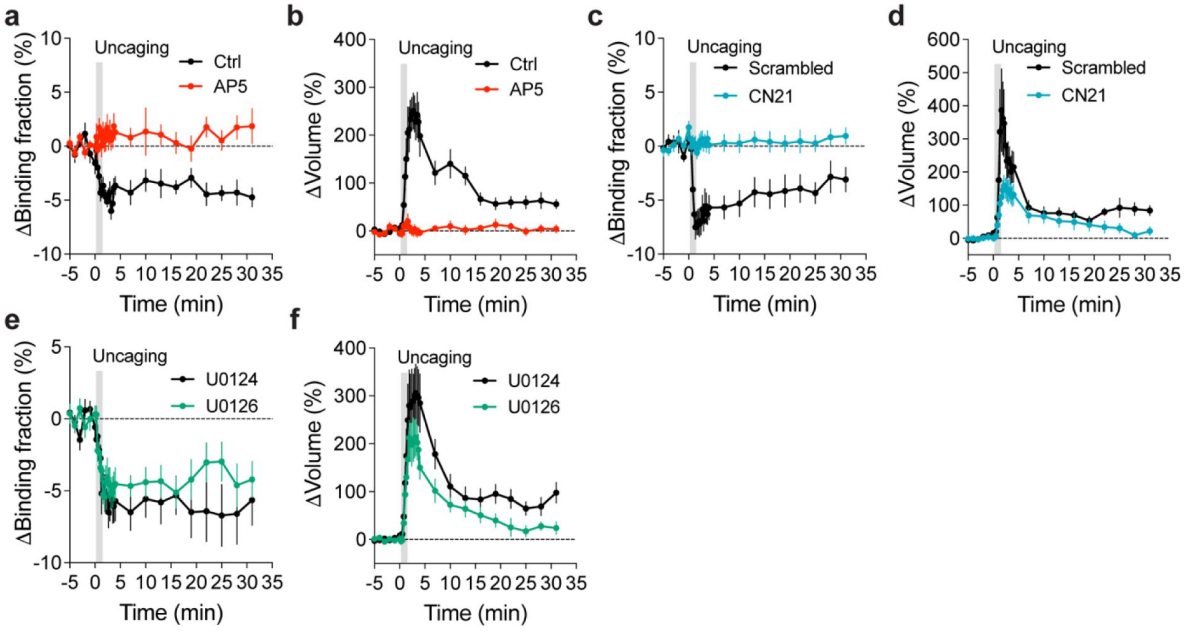

Extended Data Fig. 7

Rab10 inactivation under manipulations of putative upstream signaling pathways.

(a and b) Averaged time courses for changes in binding fraction of Rab10 sensor (a) and volume (b) of the stimulated spines during sLTP. Black and red curves represent control (Ctrl) and AP5 (50 μM), respectively. Data represent mean ± SEM. N=15/14 and 13/11 (spine/neuron) for Ctrl and AP5, respectively. **(c and d)** Averaged time courses for changes in binding fraction of Rab10 sensor (c) and volume (d) of the stimulated spines during sLTP. Black and blue curves represent scrambled peptide control (10 μM) and CN21 peptide (10 μM), respectively. Data represent mean ± SEM. N=8/7 and 15/12 (spine/neuron) for scrambled peptide and CN21 peptide, respectively. **(e and f)** Averaged time courses for changes in binding fraction of Rab10 sensor (e) and volume (f) of the stimulated spines during sLTP. Black and green curves represent U0124 control (20 μM) and U0126 (20 μM), respectively. Data represent mean ± SEM. N=9/8 and 11/8 (spine/neuron) for U0124 and U0126, respectively. For all pharmacological inhibition experiments, hippocampal slices were incubated in the indicated drugs for 30 min before experiments. All experiments were paired with controls from neurons in the same batch of slices.

Extended Data Fig. 8

Changes in the binding fraction of mEGFP-Rab4 paired with false acceptor during sLTP.

(a) Averaged time course of changes in binding fraction of Rab4 sensor (Ctrl, black) in the stimulated spines during sLTP. When mEGFP-Rab4 was paired with a false acceptor (False, red), mCherry-Rim1 [20-227]-mCherry, little activity change was observed. Data represent mean ± SEM. N=6/5 (spine/neuron) for Ctrl, and 12/9 for False. **(b)** Quantification of changes in binding fraction in the transient phase (1.3-4 min) and sustained phase (19-31 min) for the same experiment as in (a). Data represent mean ± SEM. Stars denote statistical significance (n.s., not significant, **** p<0.0001, Student's t-tests). **(c)** Averaged time courses of spine volume changes for the same experiments as in (a). **(d)** Quantification of changes in spine volume in the transient phase (1.3-4 min) and sustained phase (19-31 min) for the same experiments as in (a). Data represent mean ± SEM (n.s., not significant, Student's t-tests). Please note the quantification data in (b) and (d) are also presented in **Fig. 3c,d,f,g**.

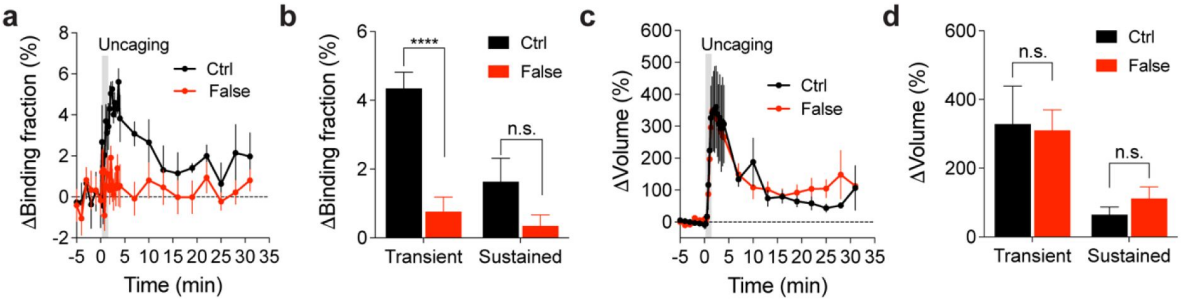

Extended Data Fig. 9

Activation of Rab4 during sLTP induction at near physiological temperature.

(a) Averaged time courses for changes in binding fraction of Rab4 sensor in the stimulated spines during sLTP at 25-27°C (black) and 33-35°C (red). Data represent mean ± SEM. N=42/34 and 16/13 (spine/neuron) for 25-27°C and 33-35°C, respectively. **(b)** Quantification of binding fraction changes in the transient phase (1.3-4 min) and sustained phase (19-31 min) for the same experiments as in (a). Data represent mean ± SEM (n.s., not significant, Student's t-tests). **(c)** Averaged time courses of changes in spine volume for the same experiments as in (a). Data represent mean ± SEM. **(d)** Quantification of spine volume changes during the transient phase (1.3-4 min) and sustained phase (19-31 min) for the same experiments as in (a). Data represent mean ± SEM (n.s., not significant, Student's t-tests). Please note that the 25-27°C (black) samples in (a-d) are the same as those in **Fig. 3b, e**.

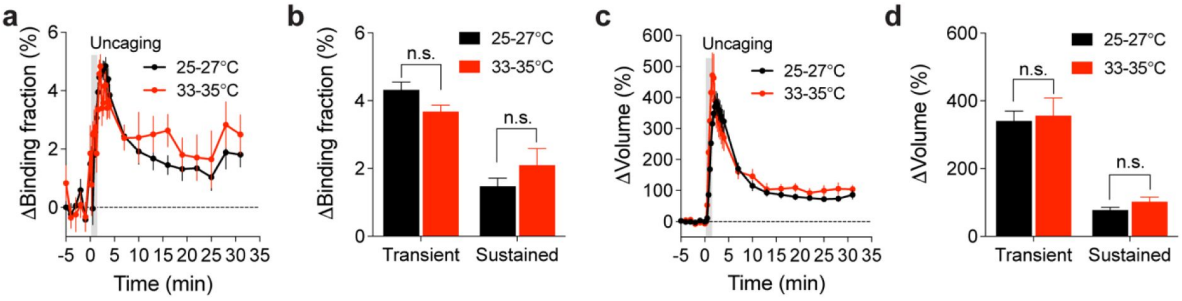

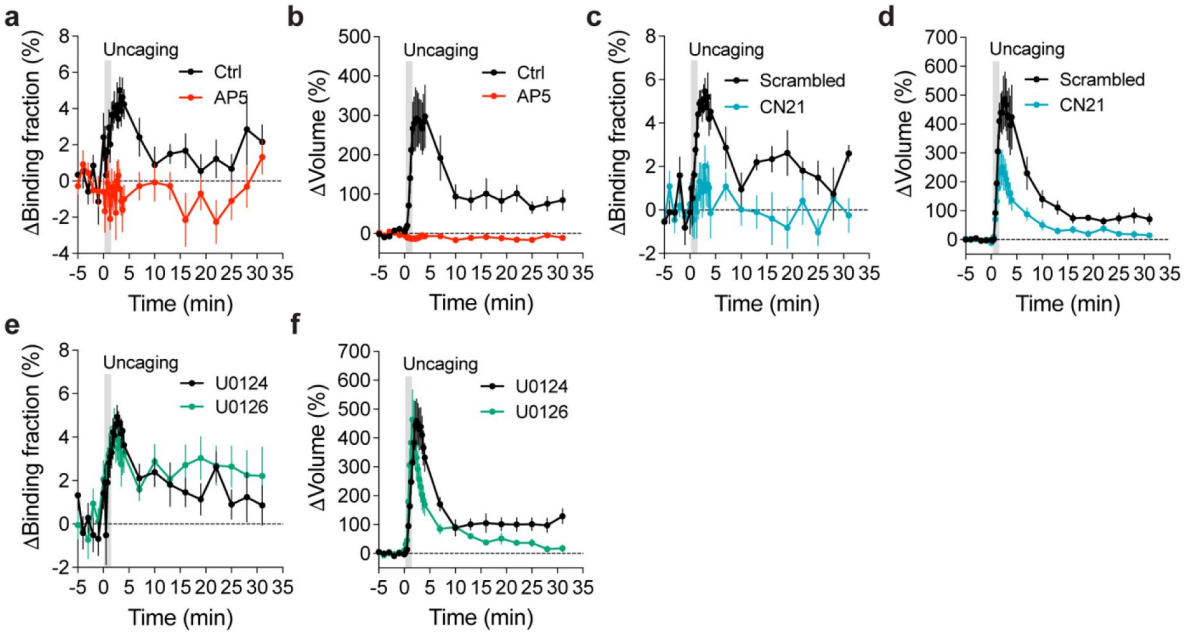

Extended Data Fig. 10

Pharmacological evaluations of upstream signaling pathways mediating Rab4 activation.

(a and b) Averaged time courses for changes in binding fraction (a) of Rab4 sensor and volume (b) of the stimulated spines during sLTP. Black and red curves represent control (Ctrl) and AP5 (50 μM), respectively. Data represent mean ± SEM. N=8/6 and 12/9 (spine/neuron) for Ctrl and AP5, respectively. **(c and d)** Averaged time courses for changes in binding fraction (c) of Rab4 sensor and volume (d) of the stimulated spines during sLTP. Black and blue curves represent scrambled peptide control (10 μM) and CN21 peptide (10 μM), respectively. Data represent mean ± SEM. N=9/8 and 13/11 (spine/neuron) for scrambled peptide and CN21 peptide, respectively. **(e and f)** Averaged time courses for changes in binding fraction of Rab4 sensor (e) and volume (f) of the stimulated spines during sLTP. Black and green curves represent U0124 control (20 μM) and U0126 (20 μM), respectively. Data represent mean ± SEM. N=10/8 and 9/8 (spine/neuron) for U0124 and U0126, respectively. For all pharmacology experiments, hippocampal slices were incubated with the indicated drugs for 30 min before experiments. All experiments were paired with control neurons from the same batch of slices.

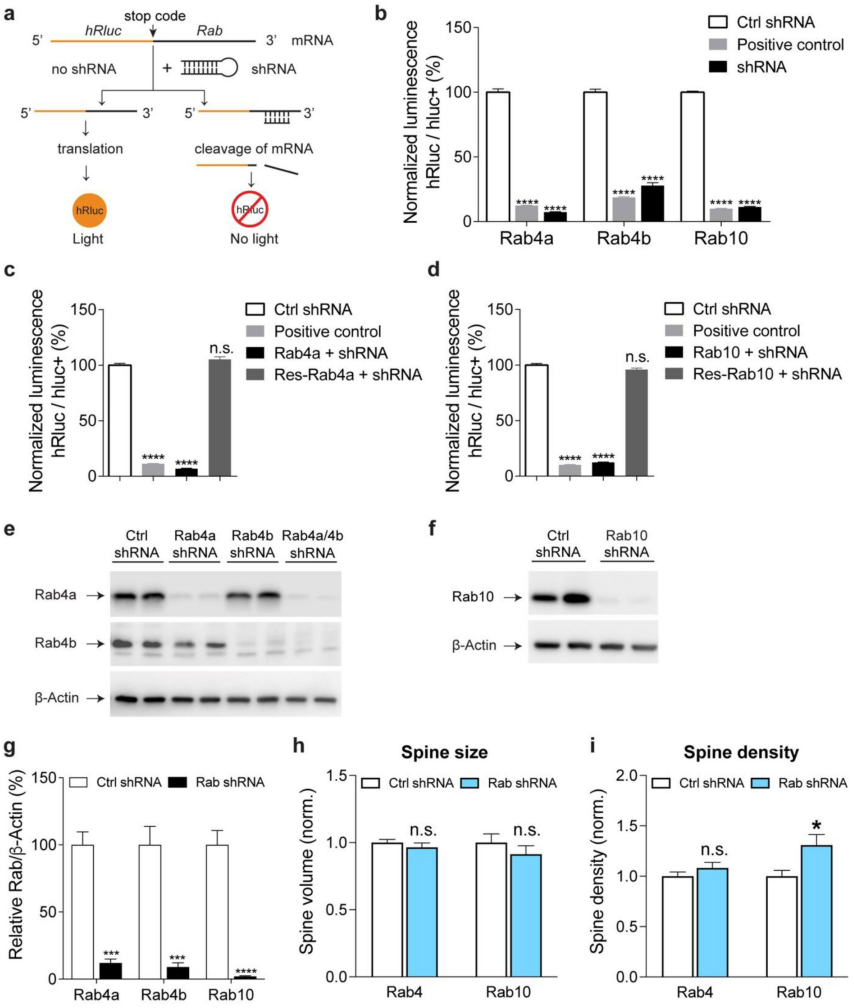

Extended Data Fig. 11

Validation of Rab GTPase shRNA and shRNA-resistant Rab GTPases, and effects of Rab knockdown on spine size and density.

(a) Schematic of dual-luciferase reporter assay. **(b)** Validation of knockdown by specific Rab4a, Rab4b and Rab10 shRNAs using dual-luciferase reporter assay. Individual psiCHECK-2-Rab GTPase was cotransfected into HEK 293T cells with scrambled shRNA (Ctrl shRNA), hRluc shRNA (Positive control) or individual Rab GTPase shRNA. Data represent mean ± SEM (**** p<0.0001, one-way ANOVA followed by Bonferroni's multiple comparison tests). N=8, 8, 8, 8, 8, 8, 10, 10, 10 wells from left to right. **(c)** Verification of shRNA-resistant Rab4a. HEK 293T cells were transfected with psiCHECK-2-shRNA-resistant Rab4a and scrambled shRNA (Ctrl shRNA), psiCHECK-2-shRNA-resistant Rab4a and hRluc shRNA (Positive control), psiCHECK-2 Rab4a and Rab4a shRNA (Rab4a+shRNA), or psiCHECK-2-shRNA-resistant Rab4a and Rab4a shRNA (Res-Rab4a+shRNA). Data represent mean ± SEM (n.s., not significant, **** p<0.0001, one-way ANOVA followed by Bonferroni's multiple comparison tests). N=4, 4, 4, 4 wells from left to right. **(d)** Verification of shRNA-resistant Rab10. HEK 293T cells were transfected with psiCHECK-2-shRNA-resistant Rab10 and scrambled shRNA (Ctrl shRNA), psiCHECK-2-shRNA-resistant Rab10 and hRluc shRNA (Positive control), psiCHECK-2 Rab10 and Rab10 shRNA (Rab10+shRNA), or psiCHECK-2-shRNA-resistant Rab10 and Rab10 shRNA (Res-Rab10+shRNA). Data represent mean ± SEM (n.s., not significant, **** p<0.0001, one-way ANOVA followed by Bonferroni's multiple comparison tests). N=5, 5, 5, 5 wells from left to right. **(e and f)** Validation of shRNA by western blot. Western blot of total protein extracts from cortical neurons cultured 15-17 days *in vitro* infected with lentiviral vectors expressing mEGFP plus either scrambled control shRNA or Rab shRNA. Data shown are representative of two independent experiments (n=4). **(g)** Quantification of the western blot experiments in (e) and (f). Data represent mean ± SEM (*** p<0.001, **** p<0.0001, Student's t-tests). **(h)** Knockdown of Rab4a/4b or Rab10 had no effect on basal spine size. Data represent mean ± SEM (n.s., not significant, Student's t-tests). N=20, 24, 20 and 20 (neurons) from left to right. **(i)** Knockdown of Rab4a/4b had no effect on spine density while knockdown of Rab10 enhanced spine density. Data represent mean ± SEM (n.s., not significant, * p<0.05, Student's t-tests). N=20, 24, 20 and 20 (neurons) from left to right.

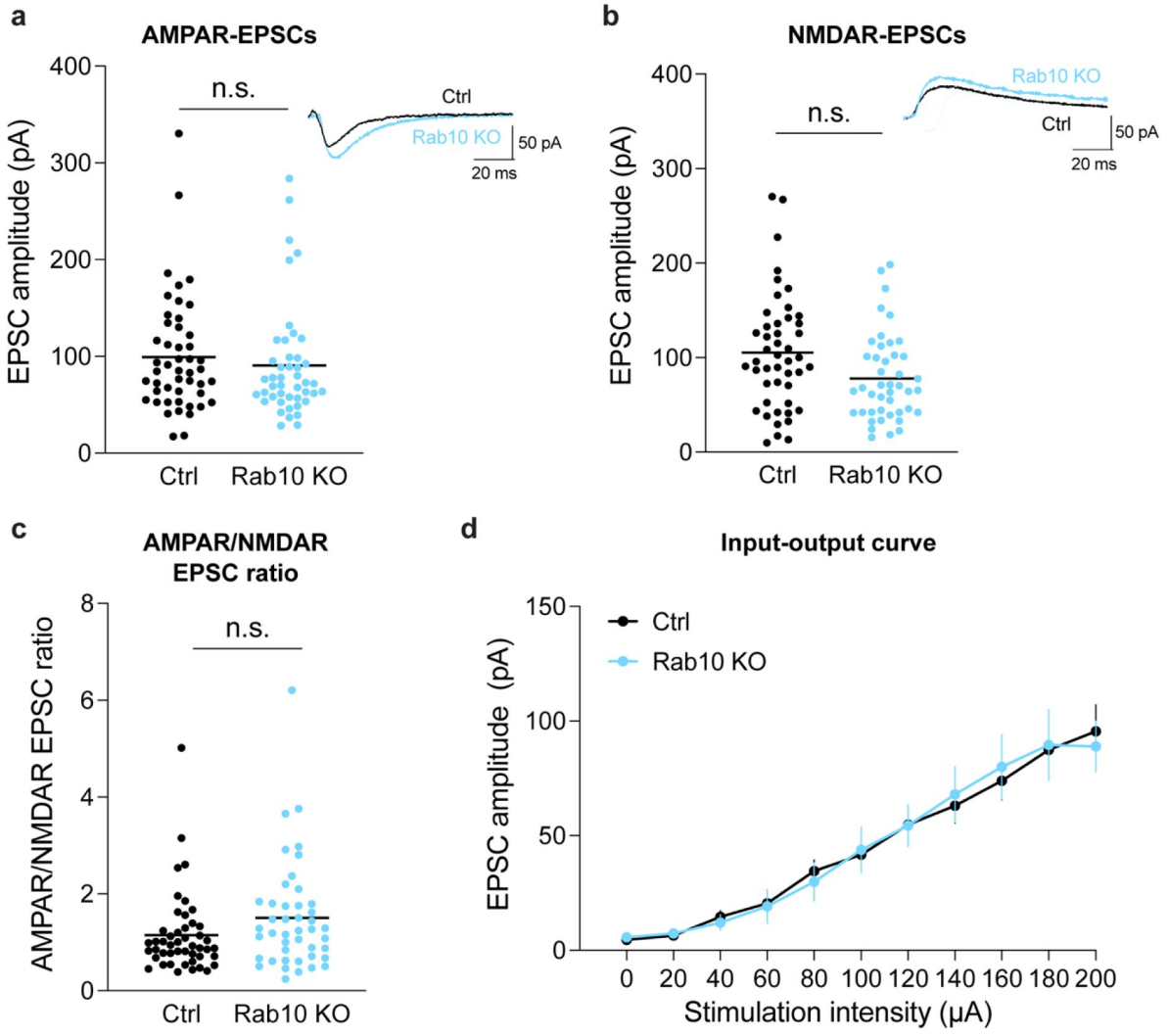

Extended Data Fig. 12

Deletion of Rab10 has no effect on CA3-CA1 synaptic transmission in the hippocampus.

(a and b) Whole cell recordings of AMPAR (a) and NMDAR (b) mediated EPSCs in *Rab10*$^{fl/fl}$:*CaMKIIα-Cre*$^{+/-}$ (Rab10 KO) mice and littermate *Rab10*$^{fl/fl}$:*CaMKIIα-Cre*$^{-/-}$ control (Ctrl) mice. **(a)** Amplitude quantification of AMPAR EPSCs (at -70mV) in Ctrl (black, n=48/5 cells/animals) and Rab10 KO (blue, n=45/5 cells/animals) mice. Insets are representative evoked responses (black for Ctrl and blue for Rab10 KO). **(b)** Amplitude quantification of NMDAR EPSCs (at +40mV) for the same experiments in (a). To avoid contamination with residual AMPAR currents, the amplitude of NMDAR EPSCs was calculated by measuring the response amplitude at 50 ms after the peak. Insets are representative evoked responses. **(c)** AMPAR/NMDAR EPSC ratio for Ctrl (black) and Rab10 KO (blue) mice. **(d)** Input-output relationship for Ctrl (black) and Rab10 KO (blue) mice. No significant difference was detected in any of the results using unpaired t-tests.

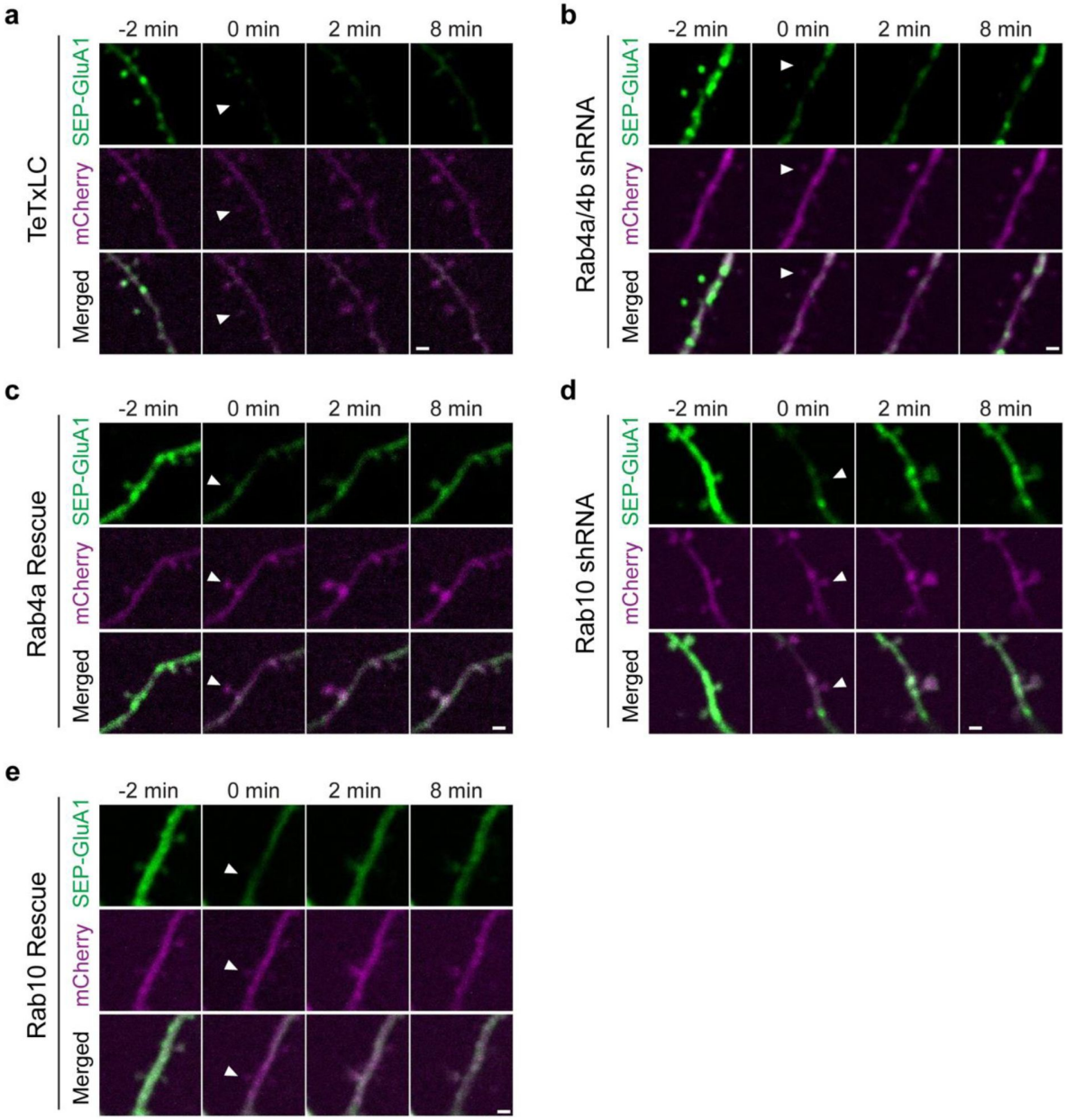

Extended Data Fig. 13

Rab4 and Rab10 regulate activity-dependent GluA1 exocytosis in the stimulated spines during sLTP.

(a-e) Representative images of SEP-GluA1 (green) FRAP after two-photon glutamate uncaging in the stimulated spines of hippocampal neurons coexpressing mCherry and TeTxLC (a); mCherry and Rab4a and Rab4b shRNAs (b); mCherry, Rab4a and Rab4b shRNAs and shRNA-resistant Rab4a (c); mCherry and Rab10 shRNA (d) or mCherry, Rab10 shRNA and shRNA-resistant Rab10 (e). White arrowheads indicate the stimulated spine. Scale bar represents 1 μm.

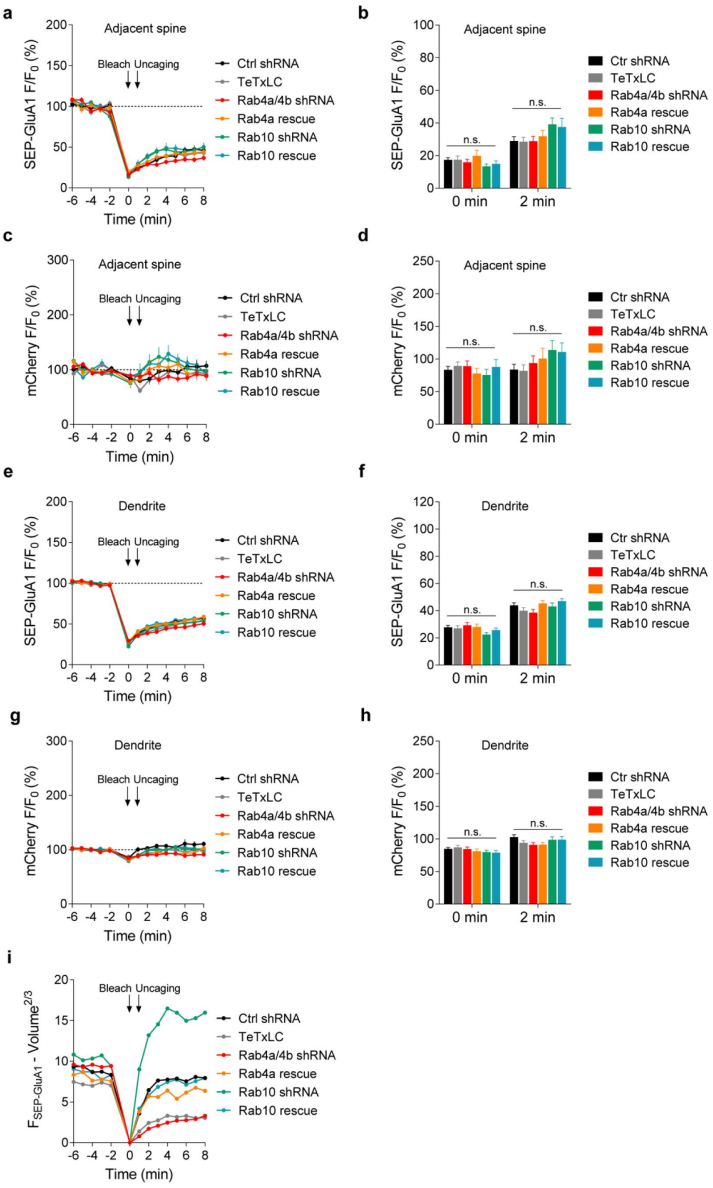

Extended Data Fig. 14

Fluorescence intensity of SEP-GluA1 and mCherry in adjacent spines and dendrites.

(a and c) Averaged time courses of SEP-GluA1 (a) and mCherry (c) fluorescence intensity for adjacent spines in the same experiments as in **Fig. 5c**. Data represent mean ± SEM. N=43/35, 19/12, 26/16, 16/12, 23/15 and 22/19 (spine/neuron) for Ctrl, TeTxLC, Rab4a/4b shRNA, Rab4a rescue, Rab10 shRNA and Rab10 rescue, respectively. **(b and d)** Quantification of SEP-GluA1 (b) and mCherry (d) fluorescence intensity for adjacent spines at 0 min and 2 min. Data represent mean ± SEM (n.s., not significant, one-way ANOVA followed by Bonferroni's multiple comparison tests). N=43/35, 19/12, 26/16, 16/12, 23/15 and 22/19 (spine/neuron) for Ctrl, TeTxLC, Rab4a/4b shRNA, Rab4a rescue, Rab10 shRNA and Rab10 rescue, respectively. **(e and g)** Averaged time courses of SEP-GluA1 (e) and mCherry (g) fluorescence intensity for dendrites in the same experiments as in **Fig. 5c**. Data represent mean ± SEM. N=43/35, 19/12, 26/16, 16/12, 23/15 and 22/19 (dendrite/neuron) for Ctrl, TeTxLC, Rab4a/4b shRNA, Rab4a rescue, Rab10 shRNA and Rab10 rescue, respectively. **(f and h)** Quantification of SEP-GluA1 (f) and mCherry (h) fluorescence intensity for dendrites at 0 min and 2 min. Data represent mean ± SEM (n.s., not significant, one-way ANOVA followed by Bonferroni's multiple comparison tests). N=43/35, 19/12, 26/16, 16/12, 23/15 and 22/19 (spine/neuron) for Ctrl, TeTxLC, Rab4a/4b shRNA, Rab4a rescue, Rab10 shRNA and Rab10 rescue, respectively. **(i)** SEP-GluA1 FRAP after subtraction of the surface area increase in the stimulated spines for experiments in **Fig. 5c**. N=43/35, 19/12, 26/16, 16/12, 23/15 and 22/19 (spine/neuron) for Ctrl, TeTxLC, Rab4a/4b shRNA, Rab4a rescue, Rab10 shRNA and Rab10 rescue, respectively.

References

1 Goto A., et al. 2021) **Stepwise synaptic plasticity events drive the early phase of memory consolidation** *Science* **374**:857–863

2 Hayashi-Takagi A., et al. 2015) **Labelling and optical erasure of synaptic memory traces in the motor cortex** *Nature* **525**:333–338

3 Matsuzaki M., Honkura N., Ellis-Davies G. C., Kasai H 2004) **Structural basis of long-term potentiation in single dendritic spines** *Nature* **429**:761–766

4 Patterson M., Yasuda R 2011) **Signalling pathways underlying structural plasticity of dendritic spines** *British journal of pharmacology* **163**:1626–1638

5 Nishiyama J., Yasuda R 2015) **Biochemical computation for spine structural plasticity** *Neuron* **87**:63–75

6 Murakoshi H., Wang H., Yasuda R 2011) **Local, persistent activation of Rho GTPases during plasticity of single dendritic spines** *Nature* **472**:100–104

7 Sun Y., Smirnov M., Kamasawa N., Yasuda R 2021) **Rapid Ultrastructural Changes in the PSD and Surrounding Membrane after induction of structural LTP in Single Dendritic Spines** *Journal of Neuroscience* **41**:7003–7014

8 Ucar H., et al. 2021) **Mechanical actions of dendritic-spine enlargement on presynaptic exocytosis** *Nature* **600**:686–689

9 Park M., et al. 2006) **Plasticity-induced growth of dendritic spines by exocytic trafficking from recycling endosomes** *Neuron* **52**:817–830

10 Park M., Penick E. C., Edwards J. G., Kauer J. A., Ehlers M. D 2004) **Recycling endosomes supply AMPA receptors for LTP** *Science* **305**:1972–1975

11 Padamsey Z., et al. 2017) **Activity-Dependent Exocytosis of Lysosomes Regulates the Structural Plasticity of Dendritic Spines** *Neuron* **93**:132–146

12 Lledo P.-M., Zhang X., Südhof T. C., Malenka R. C., Nicoll R. A 1998) **Postsynaptic membrane fusion and long-term potentiation** *Science* **279**:399–403

13 Harward S. C., et al. 2016) **Autocrine BDNF–TrkB signalling within a single dendritic spine** *Nature* **538**:99–103

14 Hayashi Y., et al. 2000) **Driving AMPA receptors into synapses by LTP and CaMKII: requirement for GluR1 and PDZ domain interaction** *Science* **287**:2262–2267

15 Huganir R. L., Nicoll R. A 2013) **AMPARs and synaptic plasticity: the last 25 years** *Neuron* **80**:704–717

16 Malinow R., Malenka R. C 2002) **AMPA receptor trafficking and synaptic plasticity** *Annual review of neuroscience* **25**:103–126

17 Sheng M., Lee S. H 2001) **AMPA receptor trafficking and the control of synaptic transmission** *Cell* **105**:825–828

18 Shi S.-H., et al. 1999) **Rapid spine delivery and redistribution of AMPA receptors after synaptic NMDA receptor activation** *Science* **284**:1811–1816

19 Kennedy M. J., Davison I. G., Robinson C. G., Ehlers M. D 2010) **Syntaxin-4 defines a domain for activity-dependent exocytosis in dendritic spines** *Cell* **141**:524–535

20 Jurado S., et al. 2013) **LTP requires a unique postsynaptic SNARE fusion machinery** *Neuron* **77**:542–558

21 Lu W.-Y., et al. 2001) **Activation of synaptic NMDA receptors induces membrane insertion of new AMPA receptors and LTP in cultured hippocampal neurons** *Neuron* **29**:243–254

22 Ahmad M., et al. 2012) **Postsynaptic complexin controls AMPA receptor exocytosis during LTP** *Neuron* **73**:260–267

23 Wang Z., et al. 2008) **Myosin Vb mobilizes recycling endosomes and AMPA receptors for postsynaptic plasticity** *Cell* **135**:535–548

24 Wu D., et al. 2017) **Postsynaptic synaptotagmins mediate AMPA receptor exocytosis during LTP** *Nature*

25 Stenmark H 2009) **Rab GTPases as coordinators of vesicle traffic** *Nature reviews Molecular cell biology* **10**:513–525

26 Zerial M., McBride H 2001) **Rab proteins as membrane organizers** *Nature reviews Molecular cell biology* **2**:107–117

27 Hutagalung A. H., Novick P. J 2011) **Role of Rab GTPases in membrane traffic and cell physiology** *Physiological reviews* **91**:119–149

28 Hausser A., Schlett K 2019) **Coordination of AMPA receptor trafficking by Rab GTPases** *Small GTPases* **10**:419–432

29 Correia S. S., et al. 2008) **Motor protein–dependent transport of AMPA receptors into spines during long-term potentiation** *Nature neuroscience* **11**:457–466

30 Brown T. C., Correia S. S., Petrok C. N., Esteban J. A 2007) **Functional compartmentalization of endosomal trafficking for the synaptic delivery of AMPA receptors during long-term potentiation** *Journal of Neuroscience* **27**:13311–13315

31 Gerges N. Z., Backos D. S., Esteban J. A 2004) **Local control of AMPA receptor trafficking at the postsynaptic terminal by a small GTPase of the Rab family** *J. Biol. Chem* **279**:43870–43878

32 Brown T. C., Tran I. C., Backos D. S., Esteban J. A 2005) **NMDA receptor-dependent activation of the small GTPase Rab5 drives the removal of synaptic AMPA receptors during hippocampal LTD** *Neuron* **45**:81–94

33 Ehlers M. D 2000) **Reinsertion or degradation of AMPA receptors determined by activity-dependent endocytic sorting** *Neuron* **28**:511–525

34 Sönnichsen B., De Renzis S., Nielsen E., Rietdorf J., Zerial M 2000) **Distinct membrane domains on endosomes in the recycling pathway visualized by multicolor imaging of Rab4, Rab5, and Rab11** *The Journal of cell biology* **149**:901–914

35 van der Sluijs P., et al. 1992) **The small GTP-binding protein rab4 controls an early sorting event on the endocytic pathway** *Cell* **70**:729–740

36 Zou W., Yadav S., DeVault L., Jan Y. N., Sherwood D. R 2015) **RAB-10-dependent membrane transport is required for dendrite arborization** *PLoS Genet* **11**:e1005484

37 Wang T., et al. 2011) **Lgl1 activation of rab10 promotes axonal membrane trafficking underlying neuronal polarization** *Developmental cell* **21**:431–444

38 Liu Y., et al. 2013) **Myosin Vb controls biogenesis of post-Golgi Rab10 carriers during axon development** *Nature communications* **4**

39 Taylor C. A., Yan J., Howell A. S., Dong X., Shen K 2015) **RAB-10 regulates dendritic branching by balancing dendritic transport** *PLoS Genet* **11**:e1005695

40 Ridge P. G., et al. 2017) **Linkage, whole genome sequence, and biological data implicate variants in RAB10 in Alzheimer's disease resilience** *Genome medicine* **9**:1–14

41 Tavana J. P., et al. 2019) **RAB10: an Alzheimer's disease resilience locus and potential drug target** *Clinical Interventions in Aging* **14**

42 Yasuda R 2006) **Imaging spatiotemporal dynamics of neuronal signaling using fluorescence resonance energy transfer and fluorescence lifetime imaging microscopy** *Current opinion in neurobiology* **16**:551–561

43 Yasuda R 2012) **Studying signal transduction in single dendritic spines** *Cold Spring Harbor perspectives in biology* **4**:a005611

44 Eathiraj S., Pan X., Ritacco C., Lambright D. G 2005) **Structural basis of family-wide Rab GTPase recognition by rabenosyn-5** *Nature* **436**:415–419

45 Fukuda M 2003) **Distinct Rab Binding Specificity of Rim1, Rim2, Rabphilin, and Noc2: IDENTIFICATION OF A CRITICAL DETERMINANT OF Rab3A/Rab27A RECOGNITION BY Rim2* 210** *J. Biol. Chem* **278**:15373–15380

46 Pankiv S., et al. 2010) **FYCO1 is a Rab7 effector that binds to LC3 and PI3P to mediate microtubule plus end–directed vesicle transport** *Journal of Cell Biology* **188**:253–269

47 Simonsen A., et al. 1998) **EEA1 links PI (3) K function to Rab5 regulation of endosome fusion** *Nature* **394**:494–498

48 Goedhart J., et al. 2012) **Structure-guided evolution of cyan fluorescent proteins towards a quantum yield of 93%** *Nature communications* **3**

49 Takahashi N., et al. 2015) **Two-photon fluorescence lifetime imaging of primed SNARE complexes in presynaptic terminals and [beta] cells** *Nature communications* **6**

50 Chamberlain M. D., Berry T. R., Pastor M. C., Anderson D. H 2004) **The p85α subunit of phosphatidylinositol 3'-kinase binds to and stimulates the GTPase activity of Rab proteins** *J. Biol. Chem* **279**:48607–48614

51 Fukuda M., Kanno E., Ishibashi K., Itoh T 2008) **Large scale screening for novel rab effectors reveals unexpected broad Rab binding specificity** *Molecular & Cellular Proteomics* **7**:1031–1042

52 Hattula K., Furuhjelm J., Arffman A. 2002) **A Rab8-specific GDP/GTP exchange factor is involved in actin remodeling and polarized membrane transport** *Molecular biology of the cell* **13**:3268–3280

53 Itoh T., Satoh M., Kanno E., Fukuda M 2006) **Screening for target Rabs of TBC (Tre-2/Bub2/Cdc16) domain-containing proteins based on their Rab-binding activity** *Genes to cells* **11**:1023–1037

54 Rink J., Ghigo E., Kalaidzidis Y., Zerial M 2005) **Rab conversion as a mechanism of progression from early to late endosomes** *Cell* **122**:735–749

55 Tall G. G., Barbieri M. A., Stahl P. D., Horazdovsky B. F 2001) **Ras-activated endocytosis is mediated by the Rab5 guanine nucleotide exchange activity of RIN1** *Developmental cell* **1**:73–82

56 Yoshimura S.-i., Gerondopoulos A., Linford A., Rigden D. J., Barr F. A. 2010) **Family-wide characterization of the DENN domain Rab GDP-GTP exchange factors** *Journal of Cell Biology* **191**:367–381

57 Hedrick N. G., et al. 2016) **Rho GTPase complementation underlies BDNF-dependent homo- and heterosynaptic plasticity** *Nature* **538**:104–108

58 Harvey C. D., Yasuda R., Zhong H., Svoboda K 2008) **The spread of Ras activity triggered by activation of a single dendritic spine** *Science* **321**:136–140

59 Mikuni T., Nishiyama J., Sun Y., Kamasawa N., Yasuda R 2016) **High-throughput, high-resolution mapping of protein localization in mammalian brain by in vivo genome editing** *Cell* **165**:1803–1817

60 Vest R. S., Davies K. D., O'Leary H., Port J. D., Bayer K. U 2007) **Dual mechanism of a natural CaMKII inhibitor** *Molecular biology of the cell* **18**:5024–5033

61 Chang B. H., Mukherji S., Soderling T. R 1998) **Characterization of a calmodulin kinase II inhibitor protein in brain** *Proceedings of the National Academy of Sciences* **95**:10890–10895

62 Lee S.-J. R., Escobedo-Lozoya Y., Szatmari E. M., Yasuda R 2009) **Activation of CaMKII in single dendritic spines during long-term potentiation** *Nature* **458**:299–304

63 Vazirani R. P., et al. 2016) **Disruption of adipose Rab10-dependent insulin signaling causes hepatic insulin resistance** *Diabetes* **65**:1577–1589

64 Chang J.-Y., et al. 2017) **CaMKII autophosphorylation is necessary for optimal integration of Ca2+ signals during LTP induction, but not maintenance** *Neuron* **94**:800–808

65 Tsien J. Z., et al. 1996) **Subregion-and cell type–restricted gene knockout in mouse brain** *Cell* **87**:1317–1326

66 Patterson M. A., Szatmari E. M., Yasuda R 2010) **AMPA receptors are exocytosed in stimulated spines and adjacent dendrites in a Ras-ERK–dependent manner during long-term potentiation** *Proceedings of the National Academy of Sciences* **107**:15951–15956

67 Makino H., Malinow R 2009) **AMPA receptor incorporation into synapses during LTP: the role of lateral movement and exocytosis** *Neuron* **64**:381–390

68 Miesenböck G., De Angelis D. A., Rothman J. E 1998) **Visualizing secretion and synaptic transmission with pH-sensitive green fluorescent proteins** *Nature* **394**:192–195

69 Link E., et al. 1992) **Tetanus toxin action: inhibition of neurotransmitter release linked to synaptobrevin proteolysis** *Biochemical and biophysical research communications* **189**:1017–1023

70 Noguchi J., Matsuzaki M., Ellis-Davies G. C., Kasai H 2005) **Spine-neck geometry determines NMDA receptor-dependent Ca 2+ signaling in dendrites** *Neuron* **46**:609–622

71 Blitzer R. D., et al. 1998) **Gating of CaMKII by cAMP-regulated protein phosphatase activity during LTP** *Science* **280**:1940–1943

72 Genoux D., et al. 2002) **Protein phosphatase 1 is a molecular constraint on learning and memory** *Nature* **418**:970–975

73 Yagishita S., et al. 2014) **A critical time window for dopamine actions on the structural plasticity of dendritic spines** *Science* **345**:1616–1620

74 Zhu J. J., Qin Y., Zhao M., Van Aelst L., Malinow R 2002) **Ras and Rap control AMPA receptor trafficking during synaptic plasticity** *Cell* **110**:443–455

75 Van der Sluijs P., et al. 1992) **Reversible phosphorylation--dephosphorylation determines the localization of rab4 during the cell cycle** *The EMBO Journal* **11**:4379

76 Steger M., et al. 2016) **Phosphoproteomics reveals that Parkinson's disease kinase LRRK2 regulates a subset of Rab GTPases** *eLife* **5**:e12813

77 Zhai S., Ark E. D., Parra-Bueno P., Yasuda R 2013) **Long-distance integration of nuclear ERK signaling triggered by activation of a few dendritic spines** *Science* **342**:1107–1111

78 Tang S., Yasuda R 2017) **Imaging ERK and PKA Activation in Single Dendritic Spines during Structural Plasticity** *Neuron*

79 Bosch M., et al. 2014) **Structural and molecular remodeling of dendritic spine substructures during long-term potentiation** *Neuron* **82**:444–459

80 Lee H., et al. 1998) **NMDA induces long-term synaptic depression and dephosphorylation of the GluR1 subunit of AMPA receptors in hippocampus** *Neuron* **21**:1151–1162

81 Stoppini L., Buchs P.-A., Muller D 1991) **A simple method for organotypic cultures of nervous tissue** *Journal of neuroscience methods* **37**:173–182

82 Shibata M., Uchihashi T., Ando T., Yasuda R 2015) **Long-tip high-speed atomic force microscopy for nanometer-scale imaging in live cells** *Scientific reports* **5**:8724

83 Kitano M., Nakaya M., Nakamura T., Nagata S., Matsuda M 2008) **Imaging of Rab5 activity identifies essential regulators for phagosome maturation** *Nature* **453**:241–245

84 Eisel U., et al. 1993) **Tetanus toxin light chain expression in Sertoli cells of transgenic mice causes alterations of the actin cytoskeleton and disrupts spermatogenesis** *The EMBO*

journal **12**:3365

85 Cong L., et al. 2013) **Multiplex genome engineering using CRISPR/Cas systems** *Science* **339**:819–823

86 McAllister A. K 2000) **Biolistic transfection of neurons** *Science Signaling* :pl1–pl1

87 Murakoshi H., Lee S.-J., Yasuda R 2008) **Highly sensitive and quantitative FRET– FLIM imaging in single dendritic spines using improved non-radiative YFP** *Brain cell biology* **36**:31–42

88 Holtmaat A. J., et al. 2005) **Transient and persistent dendritic spines in the neocortex in vivo** *Neuron* **45**:279–291

89 Nimchinsky E. A., Yasuda R., Oertner T. G., Svoboda K 2004) **The number of glutamate receptors opened by synaptic stimulation in single hippocampal spines** *The Journal of neuroscience* **24**:2054–2064

90 Ran F., et al. 2013) **Genome engineering using the CRISPR-Cas9 system** *Nature protocols* **8**:2281–2308

91. Lanzetti L 2007) **Actin in membrane trafficking** *Current opinion in cell biology* **19**:453–458

Author information

Jie Wang
Department of Neurobiology, Duke University School of Medicine, Durham, United States, Neuronal Signal Transduction Group, Max Planck Florida Institute for Neuroscience, Jupiter, United States, Division of Life Science, The Hong Kong University of Science and Technology, Hong Kong, China

Jun Nishiyama
Neuronal Signal Transduction Group, Max Planck Florida Institute for Neuroscience, Jupiter, United States, Program in Neuroscience and Behavioral Disorders, Duke-NUS Medical School, Singapore, Singapore
ORCID iD: 0000-0002-3627-8114

Paula Parra-Bueno
Neuronal Signal Transduction Group, Max Planck Florida Institute for Neuroscience, Jupiter, United States

Elwy Okaz
Neuronal Signal Transduction Group, Max Planck Florida Institute for Neuroscience, Jupiter, United States

Goksu Oz
Neuronal Signal Transduction Group, Max Planck Florida Institute for Neuroscience, Jupiter, United States

Xiaodan Liu
Neuronal Signal Transduction Group, Max Planck Florida Institute for Neuroscience, Jupiter, United States

Tetsuya Watabe
Neuronal Signal Transduction Group, Max Planck Florida Institute for Neuroscience, Jupiter, United States

Irena Suponitsky-Kroyter
Neuronal Signal Transduction Group, Max Planck Florida Institute for Neuroscience, Jupiter, United States

Timothy E McGraw
Weill Cornell Medicine Graduate School of Medical Sciences, New York, United States

Erzsebet M Szatmari
Neuronal Signal Transduction Group, Max Planck Florida Institute for Neuroscience, Jupiter, United States, Department of Physical Therapy, East Carolina University, Greenville, United States

Ryohei Yasuda
Neuronal Signal Transduction Group, Max Planck Florida Institute for Neuroscience, Jupiter, United States
ORCID iD: 0000-0001-6263-9297

For correspondence: ryohei.yasuda@mpfi.org

Editors

Reviewing Editor
Sacha Nelson
Brandeis University, Waltham, United States of America

Senior Editor
Sacha Nelson
Brandeis University, Waltham, United States of America

Reviewer #1 (Public review):

Summary:

Wang et al. created a series of specific FLIM-FRET sensors to measure the activity of different Rab proteins in small cellular compartments. They apply the new sensors to monitor Rab activity in dendritic spines during induction of LTP. They find sustained (30 min) inactivation of Rab10 and transient (5 min) activation of Rab4 after glutamate uncaging in zero Mg. NMDAR function and CaMKII activation are required for these effects. Knock-down of Rab4 reduced spine volume change while knock-down of Rab10 boosted it and enhanced functional LTP (in KO mice). To test Rab effects on AMPA receptor exocytosis, the authors performed FRAP of fluorescently labeled GluA1 subunits in the plasma membrane. Within 2-3 min, new AMPARs appear on the surface via exocytosis. This process is accelerated by Rab10 knock-down and slowed by Rab4 knock-down. The authors conclude that CaMKII promotes

AMPAR exocytosis by i) activating Rab4, the exocytosis driver and ii) inhibiting Rab10, possibly involved in AMPAR degradation.

Strengths:

The work is a technical tour de force, adding fundamental insights to our understanding of the crucial functions of different Rab proteins in promoting/preventing synaptic plasticity. The complexity of compartmentalized Ras signaling is poorly understood and this study makes substantial inroads. The new sensors are thoroughly characterized, seem to work very well and will be quite useful for the neuroscience community and beyond (e.g. cancer research). The use of FLIM for read-out is compelling for precise activity measurements in rapidly expanding compartments (i.e., spines during LTP). In addition to structural changes, evidence for functional LTP is provided, too.

Weaknesses:

The interpretation of the FRAP experiments (Fig. 5, Ext. Data Fig. 13) is not straightforward as spine volume and surface area greatly expand during uncaging. I appreciate the correction for added spine membrane shown in Extended Data Fig. 14i.
Pharmacological experiments were not conducted or analyzed blind, risking bias in the selection/exclusion of experiments for analysis.

https://doi.org/10.7554/eLife.103879.2.sa3

Reviewer #2 (Public review):

Summary:

Wang et al. developed a set of optical sensors to monitor Rab protein activity. Their investigation into Rab activity in dendritic spines during structural long-term plasticity (sLTP) revealed sustained Rab10 inactivation (>30min) and transient Rab4 activation (~5 min). Through pharmacological and genetic manipulation to constitutively activate or inhibit Rab proteins, the authors discovered that Rab10 negatively regulates sLTP and AMPA receptor trafficking, while Rab4 positively influences sLTP but only during the transient phase. These optical sensors provide new tools for studying Rab activity in cell biology and neurobiology. The distinct kinetics and functions of Rab proteins are important for understanding synaptic plasticity. However, there are some concerns regarding result inconsistencies within this manuscript and with prior work.

Strengths:

(1) The introduction of a series of novel sensors that can address numerous questions in Rab biology.
(2) The use of multiple methods to manipulate Rab proteins to reveal the roles of Rab10 and Rab4 in LTP.
(3) The discovery of Rab4 activation and Rab10 inhibition with different kinetics during sLTP, correlating with their functional roles in the transient (Rab4) and both transient and sustained (Rab10) phases of sLTP.

Weaknesses:

(1) The discrepancy between spine phenotype and sLTP potential with Rab10 perturbation remains unexplained (refer to previous Weakness #4). The basal state is the outcome of many activity-dependent processes that are physiologically relevant. It is also unclear why different preparations would yield different results. These can be experimentally addressed, and it is at least important to highlight and discuss the discrepancies.

(2) In the response, the authors estimated that the bleed-through from mEGFP-Rab is ~3% and the red channel signal from FRET changes is ~20%. The context of these percentages is unclear. Are they percentages of the total signal in the red channel, or does 3% refer to 3% of the green channel signal? Additionally, there is no explanation of how these numbers were estimated.
(3) The changes in the fEPSP slope in response to theta burst stimulation (a decrease followed by a gradual increase) differ from prior publications (e.g. PMID: 1359925, 3967730, 19144965, 20016099). The explanation of these differences due to different conditions in response to Reviewer's recommendation #6 does not seem sufficient.

https://doi.org/10.7554/eLife.103879.2.sa2

Reviewer #3 (Public review):

Summary:

This study examines the roles of Rab10 and Rab4 proteins in structural long-term potentiation (sLTP) and AMPA receptor (AMPAR) trafficking in hippocampal dendritic spines using various different methods and organotypic slice cultures as the biological model.
The paper shows that Rab10 inactivation enhances AMPAR insertion and dendritic spine head volume increase during sLTP, while Rab4 supports the initial stages of these processes.
The key contribution of this study is identifying Rab10 inactivation as a previously unknown facilitator of AMPAR insertion and spine growth, acting as a brake on sLTP when active. Rab4 and Rab10 seems to be playing opposing roles, suggesting a somewhat coordinated mechanism that precisely controls synaptic potentiation, with Rab4 facilitating early changes and Rab10 restricting the extent and timing of synaptic strengthening.

Strengths:

The study combines multiple techniques such as FRET/FLIM imaging, pharmacology, genetic manipulations and electrophysiology to dissect the roles of Rab10 and Rab4 in sLTP. The authors developed highly sensitive FRET/FLIM-based sensors to monitor Rab protein activity in single dendritic spines. This allowed them to study the spatiotemporal dynamics of Rab10 and Rab4 activity during glutamate uncaging induced sLTP. They also developed various controls to ensure the specificity of their observations. For example, they used a false acceptor sensor to verify the specificity of the Rab10 sensor response.

This study reveals previously unknown roles for Rab10 and Rab4 in synaptic plasticity, showing their opposing functions in regulating AMPAR trafficking and spine structural plasticity during LTP.

Weaknesses:

In the first round of revision I raised these points:

(1) In sLTP, the initial volume of stimulated spines is an important determinant of induced plasticity. To address changes in initial volume and those induced by uncaging, the authors present Extended Data Figure 2. In my view, the methods of fitting, sample selection, or both may pose significant limitations for interpreting the overall results. While the initial spine size distribution for Rab10 experiments spans ~0.1-0.4 fL (with an unusually large single spine at the upper end), Rab4 spine distribution spans a broader range of ~0.1-0.9 fL. If the authors applied initial size-matched data selection or used polynomial rather than linear fitting, panels a, b, e, f, and g might display a different pattern. In that case, clustering analysis based on initial size may be necessary to enable a fair comparison between groups-not only for this figure but also for main Figures 2 and 3.

- The authors responded to this point as follows: For sensor uncaging experiments, we usually uncaged glutamate at large mushroom spines because we need to have a good signal-to-noise ratio. We just happen to choose these spines with different initial sizes for Rab4 sensor and Rab10 sensor uncaging experiments.

Even if they happen to choose these spine sizes, it is possible to compare only those that match in size. This does not require any additional experiments. Because of this, I do not find this response satisfactory.

(2) Another limitation is the absence of in vivo validation, as the experiments were performed in organotypic hippocampal slices, which may not fully replicate the complexity of synaptic plasticity in an intact brain, where excitatory and inhibitory processes occur concurrently. High concentrations of MNI-glutamate (4 mM in this study) are known to block GABAergic responses due to its antagonistic effect on GABA-A receptors, thereby precluding the study of inhibitory network activity or connectivity, which is already known to be altered in organotypic slice cultures.

- I found the Authors following response reasonable and useful:

We appreciate the reviewer's comments and would like to clarify that we have conducted experiments in acute slices for LTP using conditional Rab10 knockout (Fig. 4k, 4l), and we obtained similar results. Additionally, we have recently published findings on the behavioral deficits observed in heterozygous Rab10 knockout mice (PubMed 37156612). These studies further support our conclusions and provide additional context for our findings.

https://doi.org/10.7554/eLife.103879.2.sa1

Author response:

The following is the authors' response to the original reviews.

> ***Reviewer #1 (Public review):***
>
> *Summary:*
>
> *Wang et al. created a series of specific FLIM-FRET sensors to measure the activity of different Rab proteins in small cellular compartments. They apply the new sensors to monitor Rab activity in dendritic spines during induction of LTP. They find sustained (30 min) inactivation of Rab10 and transient (5 min) activation of Rab4 after glutamate uncaging in zero Mg. NMDAR function and CaMKII activation are required for these effects. Knockdown of Rab4 reduced spine volume change while knockdown of Rab10 boosted it and enhanced functional LTP (in KO mice). To test Rab effects on AMPA receptor exocytosis, the authors performed FRAP of fluorescently labeled GluA1 subunits in the plasma membrane. Within 2-3 min, new AMPARs appear on the surface via exocytosis. This process is accelerated by Rab10 knock-down and slowed by Rab4 knock-down. The authors conclude that CaMKII promotes AMPAR exocytosis by i) activating Rab4, the exocytosis driver and ii) inhibiting Rab10, possibly involved in AMPAR degradation.*
>
> *Strengths:*
>
> *The work is a technical tour de force, adding fundamental insights to our understanding of the crucial functions of different Rab proteins in promoting/preventing synaptic plasticity. The complexity of compartmentalized Ras signaling is poorly understood and this study makes substantial inroads. The new sensors are thoroughly characterized,*

> *seem to work very well, and will be quite useful for the neuroscience community and beyond (e.g. cancer research). The use of FLIM for read-out is compelling for precise activity measurements in rapidly expanding compartments (i.e., spines during LTP).*

Thank you for the evaluation.

> *Weaknesses:*
>
> *The interpretation of the FRAP experiments (Figure 5, Ext. Data Figure 13) is not straightforward as spine volume and surface area greatly expand during uncaging. I appreciate the correction for the added spine membrane shown in Extended Data Figure 14i, but shouldn't this be a correction factor (multiplication) derived from the volume increase instead of a subtraction?*

We thank the reviewer for this question. The fluorescence change should reflect a subtraction of surface area, as SEP-GluA1 is only fluorescent on the cell surface, unlike cytosolic mCherry, whose fluorescence intensity is proportional to spine volume. Therefore, the overall fluorescence change (ΔF) should be the addition of the contribution from AMPAR trafficking (ΔF_t) and the change in surface area (ΔS) multiplied by the remaining SEP-GluA1 fluorescence per unit area (f):

$$\Delta F = \Delta F_t + f\Delta S$$

Since fluorescence immediately after photobleaching (before AMPAR trafficking happens), F_0, is given by fS (S is the surface area of the spine):

$$\Delta F/F_o = \Delta F_t / F_0 + f\Delta S / fS$$

$$= \Delta F_t/fS + \Delta S/S$$

Assuming that the surface area change ($\Delta S/S$) is the volume change ($\Delta V/V$) to the power of 2/3, the contribution of the AMPAR trafficking can be calculated as:

$$\Delta F_t/F = \Delta F/F - (\Delta^{V/V})^{2/3}$$

This is the reason that we subtracted the contribution of the spine surface area. We have discussed this in the updated method section.

> *Also, experiments were not conducted or analyzed blind, risking bias in the selection/exclusion of experiments for analysis. This reduces my confidence in the results.*

We acknowledge the reviewer's concern regarding the lack of blinding in our experiments. However, it is challenging to conduct blinded experiments for certain types of studies, such as sensor screening for a protein family, where we do not have expected results or a specific hypothesis prior to the experiments. In these cases, our primary readout is whether the sensor indicates any activity change upon stimulation.

To address this concern, after identifying that Rab10 is inactivated during structural LTP (sLTP) and is likely important for inhibiting spine structural LTP, we performed blinded electrophysiology experiments and obtained similar results (deletion of Rab10 from Camk2a-positive neurons leads to enhanced LTP; Fig. 4k, 4l).

> ***Reviewer #2 (Public review):***
>
> *Summary:*

> *Wang et al. developed a set of optical sensors to monitor Rab protein activity. Their investigation into Rab activity in dendritic spines during structural long-term plasticity (sLTP) revealed sustained Rab10 inactivation (>30min) and transient Rab4 activation (~5 min). Through pharmacological and genetic manipulation to constitutively activate or inhibit Rab proteins, they found that Rab10 negatively regulates sLTP and AMPA receptor insertion, while Rab4 positively influences sLTP but only in the transient phase. The optical sensors provide new tools for studying Rab activity in cells and neurobiology. However, a full understanding of the timing of Rab activity will require a detailed characterization of sensor kinetics.*
>
> *Strengths:*
>
> *(1) Introduction of a series of novel sensors that can address numerous questions in Rab biology.*
>
> *(2) Multiple methods to manipulate Rab proteins to reveal the roles of Rab10 and rab4 in LTP.*
>
> *(3) Discovery of Rab4 activation and Rab10 inhibition with different kinetics during sLTP, correlating with their functional roles in the transient (Rab4) and both transient and sustained (Rab10) phases of sLTP.*

Thank you for the positive evaluation.

> *Weaknesses:*
>
> *(1) Lack of characterization of sensor kinetics, making it difficult to determine if the observed Rab kinetics during sLTP were due to sensor behavior or actual Rab activity.*

We estimated that the kinetics of the sensors for Rab4 and Rab10 are within a few minutes. For Rab4, we observed rapid increase and decrease of the activation in response to glutamate uncaging. Thus, this would be the upper limit of the ON/OFF time constants of Rab4. For Rab10, we observed a rapid dissociation of the sensor in response to sLTP induction within ~1 min. This means that the donor and acceptor molecules are quickly dissociated during the process. Thus, the off kinetics of the sensor is within the range of minute. Meanwhile, we have the on-kinetics from Rab10 activation (donor/accepter association) in response to NMDA application and again this is within a few minutes. Given these rapid sensor kinetics in neurons, our observation of the sustained inactivation of Rab10 should reflect the true behavior of Rab10, rather than just the sensor's response.

We revised our manuscript discussion session as follows:

"Understanding the kinetics of Rab4 and Rab10 sensors is essential for interpreting their actual activity during sLTP. The Rab4 sensor exhibits a rapid rise and fall in activation (Fig. 3), indicating ON/OFF times of less than a few minutes. In contrast, the Rab10 sensor rapidly dissociates during sLTP induction (Fig. 2), with OFF kinetics occurring within one minute and fast ON kinetics in response to NMDA (Fig. 1j). Given these rapid kinetics, the observed sustained inactivation of Rab10 likely reflects its true behavior rather than sensor dynamics."

> *(2) It is crucial to assess whether the overexpression of Rab proteins as reporters, affects Rab activity and cellular structure and physiology (e.g. spine number and size).*

While we did not measure the effects of Rab sensor overexpression on Rab activity or cellular structure and physiology, we showed that sLTP is similar in neurons expressing sensors. This suggests that the overexpression of Rab sensors does not significantly disrupt signaling required for sLTP.

> *(3) The paper does not explain the apparently different results between NMDA receptor activation and glutamate uncaging. NMDA receptor activation increased Rab10 activity, while glutamate uncaging decreased it. NMDA receptor activation resulted in sustained Rab4 activation, whereas glutamate uncaging caused only brief activation of about 5 minutes. A potential explanation, ideally supported by data, is needed.*

It is a long-standing question in the field why simple NMDA receptor activation by bath application of NMDA does not induce LTP, but instead induce LTD. Rab proteins are regulated by many GEFs and GAPs and identifying different mechanisms requires completely different techniques, such as molecular screening. While our manuscript provides some insights into this question by showing that they provide opposing signals for Rab10, we believe that identifying exact mechanisms would be out of the scope of this manuscript.

> *(4) There is a discrepancy between spine phenotype and sLTP potential with Rab10 perturbation. Rab10 perturbation affected spine density but not size, suggesting a role in spinogenesis rather than sLTP. However, glutamate uncaging affected sLTP, and spinogenesis was not examined. Explaining the discrepancy between spine size and sLTP potential is necessary. Exploring spinogenesis with glutamate uncaging would strengthen these results. Additionally, Figure 4j shows no change in synaptic transmission with Rab10 knockout, despite an increase in spine density. An explanation, ideally supported by data, is needed for the unchanged fEPSP slope despite an increase in spine density.*

We thank the reviewer for raising these important questions. In our findings, shRNA-mediated knockdown of Rab10 did not alter spine size but did increase spine density in the basal state (Extended Data Fig. 11i). This suggests that Rab10 may restrict spinogenesis without affecting spine size. Conversely, sLTP induction via glutamate uncaging is an activity-dependent process that may involve different molecular mechanisms. The signal interplay between spinogenesis and sLTP and how the exact roles of Rab signaling in different modalities of plasticity would remain elusive for the future study.

The lack of change in synaptic transmission with Rab10 knockout, despite the increase in spine density from Rab10 shRNA knockdown, may be due to different preparation and developmental stages: spine density measurements were conducted with shRNA knockdown in organotypic slices (sliced at P6-8, DIV 9-13), while electrophysiological recordings were performed in knockout mice in acute slices from adult animals (P30-60).

> *(5) Spine volume was imaged using acceptor fluorophores (mCherry, or mCherry/Venus) at 920nm, where the two-photon cross-section of mCherry is minimal. 920nm was also used to excite the donor fluorophore, hence the spine volume measurement based on total red channel fluorescence is the sum of minimal mCherry fluorescence from direct 920nm excitation, bleed-through from the green channel, and FRET. This confounded measurement requires correction and clarification.*

We assumed that the most of fluorescence is from direct excitation of mCherry at 920 nm. The contribution from the bleed-through from mEGFP-Rab (~3%) and from FRET changes (~20%) may influence the volume measurements. However, since we observed similar fluorescence changes in the green and red channels, these factors would have only a minor impact on our results (Extended Data Fig. 6a, 6d). Also, please note that the volume change in neurons expressing sensors is just to check if the volume change is normal, and not a major point of this manuscript. We clarified this in the method section as:

“For the sensor experiments, we used mCherry as a volume indicator. We acknowledge that contributions from bleed-through from mEGFP-Rab (approximately 3%) and FRET changes

(around 20%) could affect the volume measurements. However, since we observed similar fluorescence changes in both the green and red channels, we believe these factors have a minimal impact on our results (Extended Data Fig. 6a, 6d)."

> ***Reviewer #3 (Public review):***
>
> *Summary:*
>
> *This study examines the roles of Rab10 and Rab4 proteins in structural long-term potentiation (sLTP) and AMPA receptor (AMPAR) trafficking in hippocampal dendritic spines using various different methods and organotypic slice cultures as the biological model.*
>
> *The paper shows that Rab10 inactivation enhances AMPAR insertion and dendritic spine head volume increase during sLTP, while Rab4 supports the initial stages of these processes. The key contribution of this study is identifying Rab10 inactivation as a previously unknown facilitator of AMPAR insertion and spine growth, acting as a brake on sLTP when active. Rab4 and Rab10 seem to be playing opposing roles, suggesting a somewhat coordinated mechanism that precisely controls synaptic potentiation, with Rab4 facilitating early changes and Rab10 restricting the extent and timing of synaptic strengthening.*
>
> *Strengths:*
>
> *The study combines multiple techniques such as FRET/FLIM imaging, pharmacology, genetic manipulations, and electrophysiology to dissect the roles of Rab10 and Rab4 in sLTP. The authors developed highly sensitive FRET/FLIM-based sensors to monitor Rab protein activity in single dendritic spines. This allowed them to study the spatiotemporal dynamics of Rab10 and Rab4 activity during glutamate uncaging-induced sLTP. They also developed various controls to ensure the specificity of their observations. For example, they used a false acceptor sensor to verify the specificity of the Rab10 sensor response.*
>
> *This study reveals previously unknown roles for Rab10 and Rab4 in synaptic plasticity, showing their opposing functions in regulating AMPAR trafficking and spine structural plasticity during LTP.*

Thank you for the positive evaluation.

> *Weaknesses:*
>
> *In sLTP, the initial volume of stimulated spines is an important determinant of induced plasticity. To address changes in initial volume and those induced by uncaging, the authors present Extended Data Figure 2. In my view, the methods of fitting, sample selection, or both may pose significant limitations for interpreting the overall results. While the initial spine size distribution for Rab10 experiments spans ~0.1-0.4 fL (with an unusually large single spine at the upper end), Rab4 spine distribution spans a broader range of ~0.1-0.9 fL. If the authors applied initial size-matched data selection or used polynomials rather than linear fitting, panels a, b, e, f, and g might display a different pattern. In that case, clustering analysis based on initial size may be necessary to enable a fair comparison between groups not only for this figure but also for main Figures 2 and 3.*

We thank the reviewer for these questions. For sensor uncaging experiments, we usually uncaged glutamate at large mushroom spines because we need to have a good signal-to-noise ratio. We just happen to choose these spines with different initial sizes for Rab4 sensor and Rab10 sensor uncaging experiments.

> *Another limitation is the absence of in vivo validation, as the experiments were performed in organotypic hippocampal slices, which may not fully replicate the complexity of synaptic plasticity in an intact brain, where excitatory and inhibitory processes occur concurrently. High concentrations of MNI-glutamate (4 mM in this study) are known to block GABAergic responses due to its antagonistic effect on GABA-A receptors, thereby precluding the study of inhibitory network activity or connectivity [1], which is already known to be altered in organotypic slice cultures.*
>
> *(1) https://www.frontiersin.org/journals/neural-circuits/articles/10.3389/neuro.04.002.2009/full*

We appreciate the reviewer's comments and would like to clarify that we have conducted experiments in acute slices for LTP using conditional Rab10 knockout (Fig. 4k, 4l), and we obtained similar results. Additionally, we have recently published findings on the behavioral deficits observed in heterozygous Rab10 knockout mice (PubMed 37156612). These studies further support our conclusions and provide additional context for our findings.

> ***Recommendations for the authors:***
>
> ***From the Senior/Reviewing Editor:***
>
> *I apologize that this took longer than intended. As you will see from the reviews there was some disagreement on several points. There was some disagreement among reviewers as to the strength of the evidence with some characterizing it as "compelling," "convincing," or "solid" while others felt the characterization of the sensors was "incomplete" and that this could have affected some of the conclusions. After extensive discussion, reviewers agreed that there was a valid concern that the conclusion that Rab10 activation is sustained could reflect a feature of the sensor. If Rab10/RBD dissociation rate were very low, and the affinity of binding were very high, this could lead to an incorrect estimate of the sustained binding due to sensor kinetics, not Rab10 activation. It was noted that this has been seen in other sensors previously (e.g. first generation PKA activity sensors), which the developers altered in later generations to increase reversibility and off kinetics of the sensor.*
>
> *There was also discussion of how this might be addressed and we would be interested in your comments on this issue. It was suggested that it might be helpful to revise Figure 2b to show binding fraction dynamics separately for each spine (to determine whether any actually return to baseline). Subsequently, clustering of these binding dynamics into two groups could be summarized in a version of Fig. 2e for each cluster. Differences in spine volume dynamics between these clusters would provide a measure of how strongly Rab10 binding correlates with spine volume. If they never go back to baseline, some extra experiments with longer post-plasticity induction (150mins instead of 35), might show if any reversible Rab10 binding exists post-LTP induction.*
>
> *An alternative suggestion was to measure the time course in the presence of a GAP or GEF, which should alter the kinetics.*

Thanks for the comments. It is important that the inactivation is observed as the dissociation of the donor and acceptor of the sensor. Thus, the fact that the sensor rapidly decreases in response to uncaging means that they have rapid off kinetics. In addition, we provide evidence of a rapid increase of Rab10 in response to NMDA application, suggesting that kinetics is also rapid. We added discussion about this in the revised manuscript as:

“Understanding the kinetics of Rab4 and Rab10 sensors is essential for interpreting their actual activity during sLTP. The Rab4 sensor exhibits a rapid rise and fall in activation (Fig. 3),

indicating ON/OFF times of just a few minutes. In contrast, the Rab10 sensor rapidly dissociates during sLTP induction (Fig. 2), with OFF kinetics occurring within one minute and fast ON kinetics in response to NMDA (Fig. 1j). Given these rapid kinetics, the observed sustained inactivation of Rab10 likely reflects its true behavior rather than sensor dynamics."

> *There was also further discussion of the nature of the "spine volume" signal, given the fact that the two-photon cross-section of mCherry is minimal at 920nm. It was suggested that this could be due to direct acceptor excitation rather than FRET, but there was agreement that further clarity on this issue would be valuable.*

We assumed that the most of fluorescence is from direct excitation of mCherry at 920 nm. The contribution from the bleed-through from mEGFP-Rab (~3%) and from FRET changes (~20%) may influence the volume measurements. However, since we observed similar fluorescence changes in the green and red channels, these factors would have only a minor impact on our results (Extended Data Fig. 6a, 6d). Also, please note that the volume change in neurons expressing sensors is just to check if the volume change is normal, and not a major point of this manuscript. We clarified this in the method section as:

"For the sensor experiments, we used mCherry as a volume indicator. We acknowledge that contributions from bleed-through from mEGFP-Rab (approximately 3%) and FRET changes (around 20%) could affect the volume measurements. However, since we observed similar fluorescence changes in both the green and red channels, we believe these factors have a minimal impact on our results (Extended Data Fig. 6a, 6d)."

> *The equations in the methods section differ from other papers by the same lab (e.g. Laviv et al, Neuron 2020, Tu et al. Sci Adv. 2023, Jain et al. Nature 2024). Please clarify which equations are correct.*

Thanks for pointing this out. In fact, some of the equations in this manuscript were wrong, and we have corrected them in the method session.

> ***Reviewer #1 (Recommendations for the authors**):*
>
> *The effects of Rab knockdown affect both spine volume expansion and AMPAR recovery in a very similar fashion. To explain this tight coupling, the authors suggest that the availability of membrane could be a limiting factor for spine enlargement. However, some Rabs are known to affect actin dynamics, which could also explain the dual effects on AMPAR exocytosis and spine enlargement. It is not easy to come up with an experiment to differentiate between these alternative explanations, as blocking actin polymerization would likely affect exocytosis, too. The authors should consider/discuss the possibility that all of the observed Ras effects result from altered actin dynamics and that the lipid bilayer is sufficiently fluid to form a minimal surface around the expanding cytoskeleton.*

Thanks for the suggestions. We included the discussion about the potential impact on the actin cytoskeleton by Rab10.

> *Typos: heterougenous, compartmantalization, chemaical, ballistically/biolistically (chose one).*

Thanks for pointing out these typos. We have corrected them in the revised manuscript.

> ***Reviewer #2 (Recommendations for the authors):***
>
> *(1) Venus shows pH sensitivity, which can be significant at synapses due to pH changes. Characterizing the pH sensitivity of the sensors is essential.*

Thanks for the suggestions. We did not measure pH dependence, but the PKa of these fluorophores has already been published. PKa for EGFP and Venus are both 6.0, and it is unlikely that it influenced our measurements.

> *(2) Presenting individual data points within all bar graphs (e.g. Fig. 2c, 2d) would enhance data transparency.*

Thanks for the suggestions. We now provide individual data points in the revised main figures.

> *(3) In Figure 1f: Rab5 GAP expression increased the binding fraction against expectations. In addition, clarifying the color scheme in Figure 1 is needed. Are GAPs supposed to be blue/green, and GEFs red/orange? Figure 1f seems to contradict this color scheme.*

Thanks for the suggestions. We clarified these issues.

> *(4) Quantification of the point spread function of the uncaging laser, response/settle time of the scan mirror during uncaging, and reason for changes in neighboring spines in many example images (e.g. Figure 2a, especially at 240 s; Figure 4a) would be important.*

The laser is controlled by Pockels cells, which changes the laser intensity with microsecond resolution. The laser is parked for milliseconds during uncaging, much longer than the settling time of the mirror (~0.1 milliseconds). The point spread function of the uncaging laser is limited by the diffraction (~0.5 um). The uncaging spot size is mostly limited by the diffusion of uncaged glutamate, but our calcium imaging and CaMKII imaging show that the signaling is induced mostly in the stimulated spines (Lee et al., 2009; Chang et al., 2017, 2019).

> *(5) Please include traces for "false" sensors in stimulated spines in Figures 2b, 2e, 3b, and 3e.*

The traces for the false sensors have been presented in Extended Data Fig. 3 and Extended Data Fig. 8.

> *(6) The traces in Figure 4k (fEPSP slope in response to theta burst stimulation, where there is a decrease in fEPSP slope followed by a gradual increase) differ from prior publications (e.g. PMID: 1359925, 3967730, 19144965, 20016099). An investigation and explanation for these differences are necessary.*

We appreciate the reviewer's comments. We performed the experiments blindly and did not try to find a condition providing control data similar to previous publications. The variations in fEPSP responses compared to prior publications may be attributed to several factors, including differences in experimental conditions such as the genetic background of the animals used, the specific protocols for theta burst stimulation, and variations in the preparation of the hippocampal slices.

> *(7) The title and text state that Rab10 inactivation promotes AMPAR insertion. It is unclear if this is a direct effect on AMPAR insertion or an indirect effect through membrane*

> *remodeling. Providing data to distinguish these possibilities or adjusting the title/text to reflect alternative interpretations would be beneficial.*

We appreciate the reviewer's feedback. To clarify, we have revised our terminology to use "AMPAR trafficking" instead of "AMPAR insertion", as it includes both insertion and other mechanisms of AMPAR movement within the cell.

> *(8) Please provide an explanation for the initial Rab10 inactivation observed in Figure 1j upon NMDA application.*

The application of NMDA in Fig. 1j is similar to the commonly used chemical LTD induction protocol. We used this broad stimulation approach to test whether our sensors could report Rab activity changes in neurons upon strong stimulation. However, it is an entirely different stimulation approach from the sLTP induction protocol, thus resulting in different sensor activity changes. We describe the phenomenon in the revised manuscript, but we believe that detailed analyses of Rab10 activation in response to NMDA application are beyond the scope of this manuscript.

> *(9) Please explain why the study focuses on Rab4 and Rab10 instead of other Rab proteins.*

During our initial screening of sensors for various Rab proteins, we observed significant activity changes in the sensors for Rab4 and Rab10 upon sLTP induction. This suggested their potential relevance in synaptic processes, leading us to focus on understanding their specific roles in structural long-term potentiation.

> ***Reviewer #3 (Recommendations for the authors**):*
>
> *(1) Although it might seem trivial, the definition of adjacent spine has not been made in the text. It would be nice to have it in the Methods section.*

We included it in the Methods section as follows:

"The adjacent spine refers to the first or second spine located next to the stimulated spine, typically positioned opposite the stimulated spine. Additionally, the size of the adjacent spine must be sufficiently large for imaging."

> *(2) The transfection method has been mentioned as "ballistic" and "biolistic" transfection. You might want to use only one term. Additionally, you can add the equipment used (Bio-rad?) and pressure (psi) in the Methods section.*

We use “biolistic” throughout the manuscript now. We also added the equipment and conditions used.

https://doi.org/10.7554/eLife.103879.2.sa0